Applied Geochemistry 86 (2017) 121–137

Contents lists available at ScienceDirect

Applied Geochemistry

journal homepage: www.elsevier.com/locate/apgeochem

The source and evolution of paleofluids responsible for secondary minerals in low-permeability Ordovician limestones of the Michigan Basin

D.C. Petts [a, *], J.K. Saso [b], L.W. Diamond [c], L. Aschwanden [c], T.A. Al [a], M. Jensen [d]

[a] Department of Earth and Environmental Sciences, University of Ottawa, Ottawa, ON K1N 6N5, Canada
[b] Department of Earth Sciences, University of New Brunswick, Fredericton, New Brunswick, Canada
[c] Rock-Water Interaction Group, Institute of Geological Sciences, University of Bern, Baltzerstrasse 3, 3012 Bern, Switzerland
[d] Nuclear Waste Management Organization, Toronto, ON M4T 2S3, Canada

ARTICLE INFO

Article history:
Received 7 July 2017
Received in revised form
14 September 2017
Accepted 16 September 2017
Available online 20 September 2017

Handling editor: Prof. M. Kersten.

Keywords:
Michigan Basin
Low-permeability rocks
Secondary minerals
Fluid–rock interaction
Fluid inclusions
Strontium isotopes
Stable isotopes

ABSTRACT

In this study we report on the source and evolution of fluids associated with secondary vein and replacement minerals in low-permeability carbonate units in the Michigan Basin. This petrogenetic information was collected using thermometric data from fluid inclusions combined with C-, O- and Sr-isotope data, and focuses on mm- or cm-wide vein and vug minerals from Ordovician limestones of the Trenton and Black River groups and Cambrian sandstones in SW Ontario, Canada.

Primary fluid inclusions in dolomite represent fluid stage I and have the highest trapping temperatures (T_{trap}) in the sedimentary succession, between 88 and 128 °C. Primary inclusions in calcite (stage II), and celestine and anhydrite (stage III), represent the final stages of secondary mineral formation and have T_{trap} values of 54–78 °C. All three stages of vein minerals formed from brines with salinities of 31–37 wt % $[CaCl_2+NaCl]_{eq}$ that were saturated in halite and methane gas at the time of mineral growth. Three subsequent stages of secondary fluid inclusions were observed in the samples (stages IV–VI), however, no secondary vein minerals formed during these stages and they are interpreted as re-mobilization and/or minor fluid ingress along grain boundaries and micro-fractures. Notably, stage IV secondary inclusions are gas-undersaturated with salinities of 32–34 wt% $[CaCl_2+NaCl]_{eq}$ and minimum T_{trap} values of 57–106 °C, and are interpreted to have formed during a Late Devonian–Mississippian regional heating event.

Secondary minerals from the Cambrian units and the Shadow Lake Formation have $\delta^{13}C$ values of −6.1 to −2.5‰ (VPDB), $\delta^{18}O$ values of +14.6 to +24.2‰ (VSMOW) and $^{87}Sr/^{86}Sr$ of 0.70975–0.71043. Relative shifts of approximately +2 to +3‰ in $\delta^{13}C$, >+4‰ in $\delta^{18}O$ and −0.002 in $^{87}Sr/^{86}Sr$ are observed upward across the boundary between the Cambrian–Shadow Lake units and the overlying Gull River Formation. Samples from the Gull River and Coboconk formations and the Trenton Group (Kirkfield, Sherman Fall and Cobourg formations) have $\delta^{13}C$ values of −1.0 to +1.9‰, $\delta^{18}O$ values of +18.9 to +28.1‰ and $^{87}Sr/^{86}Sr$ values of 0.70790–0.70990.

The combined microthermometric and isotopic data for secondary minerals in the Cambrian–Shadow Lake units suggest they formed from hydrothermal brine with a geochemical signature obtained by interaction with the underlying Precambrian shield, or shield-derived minerals in the Cambrian sandstones. Previous U-Pb dating of vein calcite and Rb-Sr dating of secondary K-feldspar from the region suggests that brine ingress occurred during the Late Ordovician–Silurian. The O- and Sr-isotope variability in vein samples from the Gull River and Coboconk formations is interpreted as localized mixing of ^{18}O-enriched, connate fluids with hydrothermal brine. In comparison, isotopic data for the Trenton Group indicate secondary mineral formation from connate fluids, sourced from ^{18}O-enriched, evolved seawater and/or modified hydrothermal brine that experienced fluid–rock interaction during transit through the underlying stratigraphy.

* Corresponding author.
E-mail address: dpetts@uOttawa.ca (D.C. Petts).

https://doi.org/10.1016/j.apgeochem.2017.09.011
0883-2927/

1. Introduction

Low-permeability sedimentary rocks have increasingly become a global focus for a wide range of environmental and geoscience studies, including nuclear waste management (Russell and Gale, 1982; Hendry et al., 2015), CO_2 sequestration (Shafeen et al., 2004; Benson and Cole, 2008) and extraction of gas from shale (Arthur and Cole, 2014). In the cases of CO_2 sequestration and extraction of gas with hydraulic fracturing, the low-permeability rocks play a critical role in limiting the upward migration of fluids that are injected or displaced. Low-permeability sedimentary rocks have been of particular interest in countries such as Canada, Switzerland, France, Belgium and Germany for the long-term storage of nuclear waste because solute transport is dominated by diffusion and the clay-rich mineralogy provides large surface areas for solute retention by sorption mechanisms. Internationally, detailed paleofluid studies have provided valuable insight into fluid sources and solute transport mechanisms (Altmann et al., 2012; Clark et al., 2013; Al et al., 2015; Mazurek and de Haller, 2017) that are essential for evaluating the long-term viability of a site for nuclear waste storage.

Low-permeability argillaceous limestones of the Trenton Group (10^{-16} to 10^{-12} m s^{-1}; Beauheim et al., 2014), in the Bruce region of the Michigan Basin (southwestern Ontario, Canada) have been identified as a potential host rock for the construction of a deep geologic repository (DGR) for low- and intermediate-level nuclear waste. The Cobourg Formation, a low-permeability, argillaceous limestone at the top of the Trenton Group occurs >650 m beneath the Bruce nuclear site and has been proposed as the repository host rock. These limestones are overlain by up to 200 m of regionally-extensive, low-permeability Ordovician shale (Intera, 2011; Beauheim et al., 2014). Detailed studies on the long-term physical and chemical stability of the surrounding rocks have focused on a wide range of stratigraphic, structural, geophysical and geochemical methods (Intera, 2011 and references therein). Previous investigations at the Bruce site have contributed valuable information on the residence time and transport mechanisms of fluids in these rocks, which include studies of porewater geochemistry and solute transport (Clark et al., 2013; Al et al., 2015), hydraulic conductivity (Beauheim et al., 2014), and mechanisms responsible for anomalous hydraulic-head profiles observed in the Trenton and Black River group limestones (Normani and Sykes, 2012; Khader and Novakowski, 2014; Neuzil and Provost, 2014; Neuzil, 2015).

Secondary minerals from veins in sedimentary rocks provide direct information on the movement of deep basin fluids. Detailed isotopic and petrographic information of secondary minerals combined with fluid inclusion temperature constraints have been utilized in paleofluid studies to differentiate between fluid sources that relate to either diagenesis/burial (Ayalon and Longstaffe, 1988), or the influx of fluids from allochthonous sources (Spencer, 1987; Davies and Smith, 2006). Detailed petrography (e.g., Taylor and Sibley, 1986) combined with thermometric data from fluid inclusions (e.g., Roedder, 1979; Goldstein, 2001) provide an understanding of the relative timing of fluid infiltration and temperature constraints during crystallization. Here, we report on the source and evolution of fluids associated with secondary mineral formation in low-permeability Ordovician limestones and Cambrian siliciclastic units in the Michigan Basin from southwestern Ontario, Canada.

Ordovician limestones of the Trenton and Black River groups, which are laterally traceable across much of the Michigan Basin and occur in sections of the Appalachian Basin, have long been a focus of paleofluid studies due to their association with hydrocarbon reservoirs in the Albion-Scipio/Stoney Point fields in south-central Michigan (e.g., Hurley and Budros, 1990; Allan and Wiggins, 1993), the Lima-Indiana field in Ohio/Indiana (e.g., Wickstrom et al., 1992) and fields of southern Ontario (Powell et al., 1984; Middleton et al., 1993; Coniglio et al., 1994; Obermajer et al., 1999). In these fields, hydrocarbon migration/reservoir formation is closely tied to the formation of hydrothermal dolomite (Allan and Wiggins, 1993), which has been suggested to form during high-temperature, fluid–rock interaction between the Ordovician limestones and upwelling hydrothermal fluids (Davies and Smith, 2006). Furthermore, C-, O- and Sr-isotope compositions of secondary minerals in southern Ontario (Harper et al., 1995; Ziegler and Longstaffe, 2000; Haeri-Ardakani et al., 2013) and central Michigan (Allan and Wiggins, 1993) have provided valuable information on the source of deep-seated fluid migrations in these regions of the basin. In the Bruce region, however, detailed paleofluid studies have largely focused on the geochemical and isotopic evolution of porewaters in the Michigan Basin sedimentary succession (Clark et al., 2010a, 2010b; 2013, 2015; Al et al., 2015). Knowledge gaps remain in the understanding of paleofluid contributions to the formation of secondary vein minerals in the Ordovician limestones, and in particular, the source and transport mechanisms that are responsible for vein-related fluid migrations in these low-permeability sedimentary rocks.

The objective of this study is to enhance the understanding of fluid residence time and migration that has been developed from previous research at the Bruce site. Detailed petrography and microthermometric data from fluid inclusions are combined with C-, O- and Sr-isotope data to determine the source and relative timing of paleofluid migrations that resulted in the formation of secondary minerals, including vein and vug infill and replacement phases. Samples were obtained from drill cores that section the entire succession of Cambrian to Devonian sedimentary rocks and the underlying Precambrian gneissic basement.

2. Geology and stratigraphy of the Michigan Basin

The Michigan Basin represents a broadly circular, ~500 km diameter intracratonic sedimentary basin located in central North America. The study area is located along the eastern margin of the basin, at the Bruce nuclear site (Fig. 1). A detailed summary of the Paleozoic bedrock units in southern Ontario is discussed in Armstrong and Carter (2010) (and references therein), a brief description of these units is provided below. At the Bruce site, the sedimentary succession reaches a maximum thickness of ~860 m. The base of this succession comprises ~17 m of Cambrian sandstone which unconformably overlies Precambrian gneissic basement. Upper Ordovician rocks disconformably overlie the Cambrian sandstones and are subdivided into the Black River and Trenton group limestones and a thick sequence of shale. The Black River Group consists of a 4–5 m thick basal unit of siltstone and minor dolostone (Shadow Lake Formation) that is overlain by ~ 75 m of variably bioturbated and fossiliferous lithographic limestone (Gull River and Coboconk formations). Overlying the Black River Group are ~110 m of mostly argillaceous limestones of the Trenton Group (subdivided into the Kirkfield, Sherman Fall and Cobourg formations). The Cobourg Formation is further subdivided into lower and upper members, which, respectively comprise ~28 m of argillaceous limestone, with minor interbeds of calcareous shale, and ~7.5 m of calcareous shale. The Cobourg Formation is capped by ~200 m of Ordovician shale which is subdivided into the Blue Mountain, Georgian Bay and Queenston formations. Overall, the Ordovician limestone–shale succession has been interpreted as initial deposition in supra-tidal/tidal flat to lagoonal marine or offshore shallow- and deep-shelf settings (Black River and Trenton groups), and open marine to shallow intertidal or supratidal

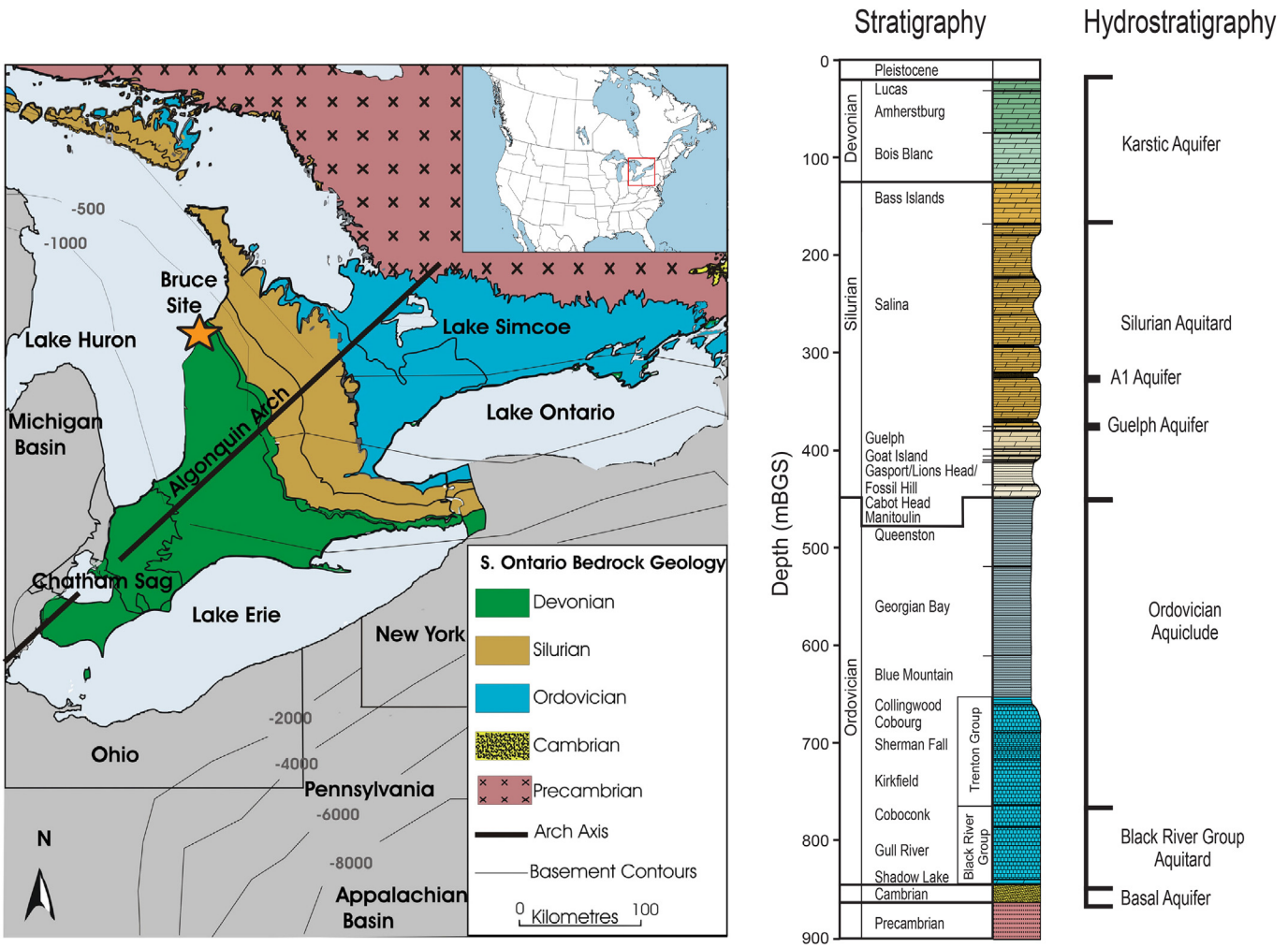

Fig. 1. Bedrock geology, stratigraphy and hydrostratigraphy of the Michigan Basin below the Bruce site, Southwestern Ontario, Canada. Also shown here are regional structural features (Algonquin Arch, Chatham Sag) and contours lines for the base of the Paleozoic sediments (i.e. elevation in metres to the top of the Precambrian basement rocks). The geologic map is based on Ontario Geological Survey (1991) and Armstrong and Carter (2010).

settings for deposition of the Blue Mountain–Queenston shales. Overlying the Ordovician shales are 415 m of Silurian and Devonian interlayered dolostone, shale and evaporitic units, which represent deposition in a carbonate-shelf setting with periods of restricted marine circulation.

Herein we refer to "Ordovician limestones", "Trenton Group limestones", "Black River Group limestones" and "Cambrian sandstones" as generalized nomenclature for each of the respective units, regardless of the minor occurrence of units/formations of differing lithology (e.g., Cambrian dolostone units, Shadow Lake siltstones/dolostones in the Black River Group, and shale in the Collingwood Member at the top of the Cobourg Formation).

Hydrogeologic conditions at the Bruce site have been investigated by Intera (2011), Normani and Sykes (2012), Beauheim et al. (2014), Khader and Novakowski (2014), Neuzil and Provost (2014) and Neuzil (2015). The objective of these studies was to understand the hydraulic properties of the sedimentary rocks through modelling (Normani and Sykes, 2012), *in situ* hydraulic conductivity measurements (Beauheim et al., 2014) and interpretation of observed anomalies in hydraulic-head distributions (Khader and Novakowski, 2014; Neuzil and Provost, 2014; Neuzil, 2015). Overall, the hydraulic data indicate that the permeability of the Upper Ordovician limestones and shales is very low, such that solute transport is limited to diffusion. *In situ* measurements of horizontal hydraulic conductivity (K_h) by Beauheim et al. (2014) indicate that the Ordovician shales and the argillaceous limestones of the Trenton Group represent an aquiclude (Fig. 1), with K_h values ranging from 10^{-16} to 10^{-12} m s^{-1}. Limestones of the Black River Group have K_h values of 10^{-12} to 10^{-10} m s^{-1} and define an aquitard (Fig. 1). The Cambrian sandstone unit has a K_h value of 10^{-6} m s^{-1} and represents a basal aquifer (Fig. 1).

3. Methods

3.1. Sampling and petrography

Samples were obtained from six drill cores (DGR-2 to DGR-6; DGR-8) at the Bruce site, and were initially collected on the basis of visible secondary minerals (calcite, dolomite, anhydrite, celestine, pyrite, halite, etc.) in veins, vugs and replacement/alteration zones, largely within the Trenton and Black River group limestones and the Cambrian sandstones. Sample depths are reported here as metres below ground surface (mBGS) relative to drill hole DGR-2.

Polished thin sections of the secondary minerals were prepared at the University of New Brunswick, and characterized using optical microscopy and electron-beam techniques (Microscopy and Microanalysis Facility at the University of New Brunswick). Secondary minerals were imaged with a JEOL 6400 scanning electron

microscope (SEM) using a backscattered electron detector (BSE) and identified using SEM-based energy-dispersive X-ray spectrometry (EDS). Quantitative measurements of major and trace element concentrations (Ca, Mg and Sr) were made using wavelength-dispersive X-ray spectrometry on a JEOL 733 Superprobe electron probe microanalyzer (EPMA), operating at 15 kV with a beam current of 15–20 nA. Integration times for each element ranged from 30 to 80 s and the detection limits were generally lower than 160 ppm for Ca and Mg, and 260 ppm for Sr.

3.2. Fluid inclusion microthermometry

Fluid inclusion measurements were undertaken in the Institute of Geological Sciences at the University of Bern, and follow the general fluid inclusion methodology outlined by Roedder (1984), Goldstein and Reynolds (1994) and Samson et al. (2003). Double-polished thick sections (150 μm) were prepared for each sample to permit characterization by optical microscopy using transmitted, plane-polarized light and reflected, ultraviolet (UV) light. UV light microscopy was utilized to identify fluid inclusions that contain hydrocarbons.

Microthermometric measurements were made using a Linkam MSD-600 heating-cooling stage mounted on an Olympus BX51 polarizing microscope. The stage was calibrated against synthetic CO_2–H_2O inclusions and synthetic H_2O inclusions with critical density, such that the accuracy is ±0.1 °C for measurements made below room temperature and ±1.0 °C for measurements above room temperature. For the microthermometric measurements of inclusions in calcite, careful attention was paid to avoid spurious data and/or anomalously high homogenization temperatures that resulted from inclusion "stretching" (i.e. deformation of the inclusion walls during heating/pressurization; Roedder and Bodnar, 1980; Goldstein and Reynolds, 1994). "Stretched" inclusions were identified by increases in the diameter of the contained vapour bubbles after heating to homogenization and cooling down to room temperature, as visible in photographs taken prior to and after heating.

Identification of gas and mineral phases trapped within the inclusions was undertaken using laser Raman spectroscopy. Either red (632.8 nm) He-Ne or green (532.12 nm) Nd-YAG lasers were focused onto the sample through an Olympus 100/0.95 UM PlanFl objective lens on a Olympus BX41 microscope, and Raman spectra were collected for 10–20 s using a Horiba Jobin-Yvon LabRam HR-800 spectrometer calibrated against the emission lines of a neon lamp.

3.3. Stable isotope analysis

C- and O-isotope measurements were conducted in the G.G. Hatch Stable Isotope Laboratory at the University of Ottawa using isotope ratio mass spectrometry (IRMS). Calcite and dolomite samples were acquired from thin section chips using a Merchantek microdrill (300 μm drill bit). Drill locations were pre-selected in portions of veins, vugs and/or alteration/replacement zones using a combination of optical microscopy and SEM-BSE imaging of the associated thin section. The powdered calcite and dolomite samples were weighed into glass reaction vessels and flushed with helium. Orthophosphoric acid was introduced into the vials and reacted for 24 h at 25 °C for calcite and 50 °C for dolomite. The C- and O-isotope ratios of the resulting CO_2 gas were measured using a Thermo-Finnigan Delta XP and Gas Bench II in continuous flow mode, and normalized against NBS-18, NBS-19 and LSVEC (carbon only). C- and O-isotope compositions are reported in δ-notation relative to Vienna Peedee belemnite (VPDB) for carbon and Vienna standard mean ocean water (VSMOW) for oxygen, in permil (‰). Analytical uncertainties associated with the $\delta^{13}C$ and $\delta^{18}O$ data are ±0.1‰ (2σ).

3.4. $^{87}Sr/^{86}Sr$ analysis

Sr-isotope ratios ($^{87}Sr/^{86}Sr$) for carbonate samples were obtained in the Isotope Geochemistry and Geochronology Research Centre (IGGRC) at Carleton University using thermal ionization mass spectrometry (TIMS). Calcite, dolomite, anhydrite and celestine samples were collected by micro-drilling following the same methodology described in Section 3.3. Sr-concentrations were determined using mean EPMA analyses for the target mineral. Samples were weighed out between 0.5 and 15 mg (depending on Sr-concentration) and dissolved in 2.5 N nitric acid. Micro-chromatography columns were prepared using 100 μL of Eichrom Sr Spec resin (5–100 μm) in a 14 mL borosilicate glass column. The resin was washed with 1200 μL of ultrapure water and then conditioned with 400 μL of 7 N nitric acid. The samples were added to the column, then washed using 7 N nitric acid. Sr ions were eluted from the resin using 1600 μL of ultrapure water, and dried down on a hot plate. The dried Sr samples were loaded onto Ta filaments using 0.3 N orthophosphoric acid and analyzed for $^{87}Sr/^{86}Sr$ using a Thermo-Finnigan Triton TIMS, at temperatures of 1300–1500 °C. Total Sr blanks for the procedure are <250 picograms. The three-year average for analyses of NIST SRM987 is $^{87}Sr/^{86}Sr = 0.710254 \pm 0.000019$. Analytical uncertainties associated with the Sr-isotope data are reported at 2σ.

4. Results

4.1. Paragenetic sequence and chemistry of secondary minerals

Secondary minerals in the Cambrian sandstones and the Black River and Trenton group limestones occur as matrix replacement and/or veins and vugs (Fig. 2). The mineral assemblages predominantly consist of calcite and dolomite, with varying proportions of anhydrite, celestine, pyrite and quartz (Fig. 3). Varying amounts of clay minerals and halite also occur as secondary minerals (Intera, 2011). Relative proportions of dolomite versus calcite (as wt% dolomite) are exhibited in Fig. 4A using bulk XRD data from Intera (2011). Elemental concentrations (Ca, Mg and Sr) are shown in Table 1S (Supporting Material).

Saddle dolomite is observed as linings in mm- or cm-wide veins and vugs within: (1) stratabound dolostone in the Sherman Fall, Coboconk, Gull River and Cambrian units, (2) Gull River limestone and (3) Shadow Lake siltstone (e.g., Fig. 2C–E, G–H; Fig. 1S – Supporting Material). Replacement dolomite occurs as fine-grained and dolomite-rich, mm- or cm-wide zones in limestone within both the Trenton and Black River groups (e.g., Fig. 2B). Uniform MgO abundances of 18–22 wt% were obtained for saddle/vein dolomite and dolostone matrix (Fig. 4B). Sr abundances are commonly less than 1000 ppm for all three types of dolomite (Fig. 4C). Dolomitic growth zones in calcite crystals (MgO up to 22 wt%) are identified in Coboconk, Gull River and Shadow Lake veins and vugs (Fig. 4B).

Secondary calcite commonly consists of medium- or coarse-grained, euhedral crystals within mm- to cm-sized veins and vugs, and are the principal vein/vug forming mineral in the Trenton and Black River groups and the Cambrian sandstones (Fig. 1S – Supporting Material). Low MgO abundances (<2 wt%) are common for most secondary calcite. Sr abundances in vein and vug calcite

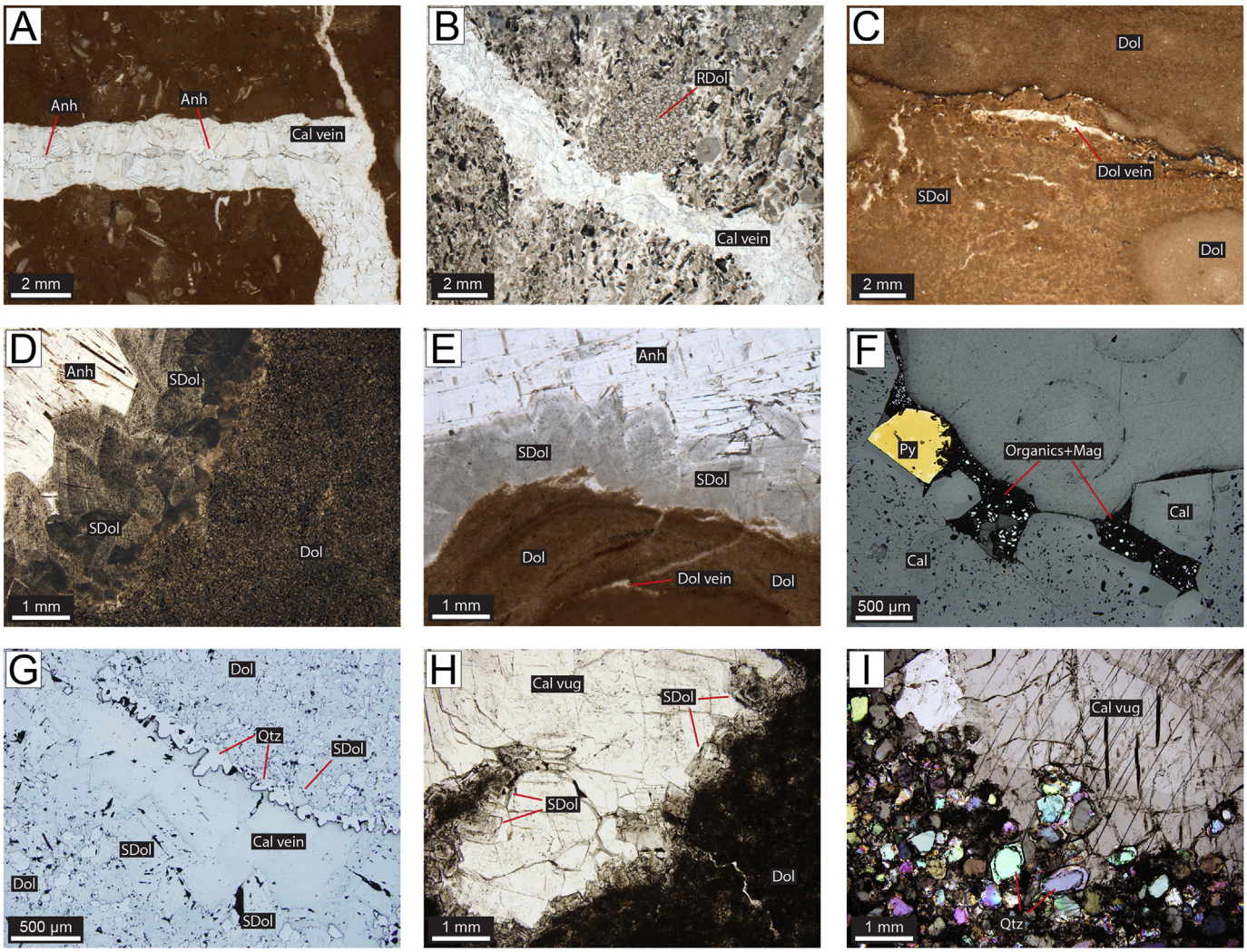

Fig. 2. Photomicrographs of secondary minerals in the Trenton Group (A–B), Black River Group (C–F) and the Cambrian units (G–I). (A) DGR-5-704.44, sharp-edged calcite vein in an argillaceous limestone, with an infill of anhydrite that post-dates calcite formation (SL); (B) DGR-2-691.70, irregular calcite vein in a fossiliferous limestone with zones of fine-grained replacement dolomite (SL); (C) DGR-2-778.44, dolostone with zones of tan saddle dolomite and discrete veins of colourless saddle dolomite (SL); (D) DGR-2-817.41, micritic limestone with a saddle dolomite vug with infill anhydrite. Note the fine-grained dolomite lining the interior of vug (PPL); (E) DGR-4-829.53, dolostone with saddle dolomite vug, infill anhydrite and discrete veins of colourless dolomite (SL); (F) DGR-2-843.83, micritic limestone with a sparry calcite vug, infill minerals include rough-edged pyrite partly replaced and followed by crystallites of magnetite suspended in an organic-rich matrix (RL); (G) DGR-4-844.78, irregular vein with saddle dolomite and quartz lining and calcite infill within a fine-grained dolostone (RL); (H) DGR-4-845.20, dolostone with saddle dolomite-lined calcite vug (PPL); (I) DGR-2-847.42, sandstone with a calcite-lined vug. Note the euhedral authigenic quartz rims that mantle detrital quartz grains (XPL). Abbreviations: Anh – anhydrite; Cal – calcite; Dol – dolomite; Mag – magnetite; PPL – plane-polarized light image; Py – pyrite; RL – reflected light image; SDol – saddle dolomite; SL – stereo-light image (combination of both transmitted and reflected light); Qtz – quartz; XPL – cross-polarized light image.

exhibit a decreasing trend with depth, from as high as 4300 ppm in the Cobourg to <950 ppm in the Cambrian (Fig. 4C).

Anhydrite and celestine are observed as late infill after saddle dolomite and calcite (Fig. 2A, D–E; Fig. 1S – Supporting Material; Saso, 2013). The abundance of Sr in anhydrite is comparable to calcite in the Cobourg and Sherman Fall formations, but it is higher than calcite in the Gull River Formation (Fig. 4C). Authigenic quartz was identified in one sandstone and one dolostone in the Cambrian, as euhedral quartz rims mantling rounded, detrital quartz cores (Fig. 2I), and druse quartz lining the wall of a calcite vein (Fig. 2G). At both of these occurrences, authigenic quartz appears to have formed either prior to or synchronous with calcite formation. In DGR-4-844.78, the quartz lining appears to postdate the growth of saddle dolomite (Fig. 2G). Pyrite is observed throughout the succession, commonly as an early matrix mineral in all limestone units (except the Sherman Fall Formation) and stratabound dolostones in the Coboconk, Gull River, and Cambrian units, and as a late vug mineral, post-dating calcite in DGR-2-843.83 (Fig. 2F).

4.2. Petrography and microthermometry of fluid inclusions

Six paleofluid stages were identified from the primary inclusions in dolomite (stage I), primary inclusions in calcite (stage II), primary inclusions in celestine and anhydrite (stage III), and secondary inclusions mostly in calcite (stages IV to VI), and are summarized in Figs. 3, 5–8 and Table 1. Photomicrographs of representative primary and secondary inclusions are shown in Figs. 5 and 6, respectively. All inclusion assemblages trapped during stages I to III contain variable proportions of liquid and methane vapour (e.g., Fig. 5B, E, H), indicating heterogeneous fluid entrapment. Therefore, trapping temperatures (T_{trap}) for these stages are defined by the minimum homogenization temperature (T_h)

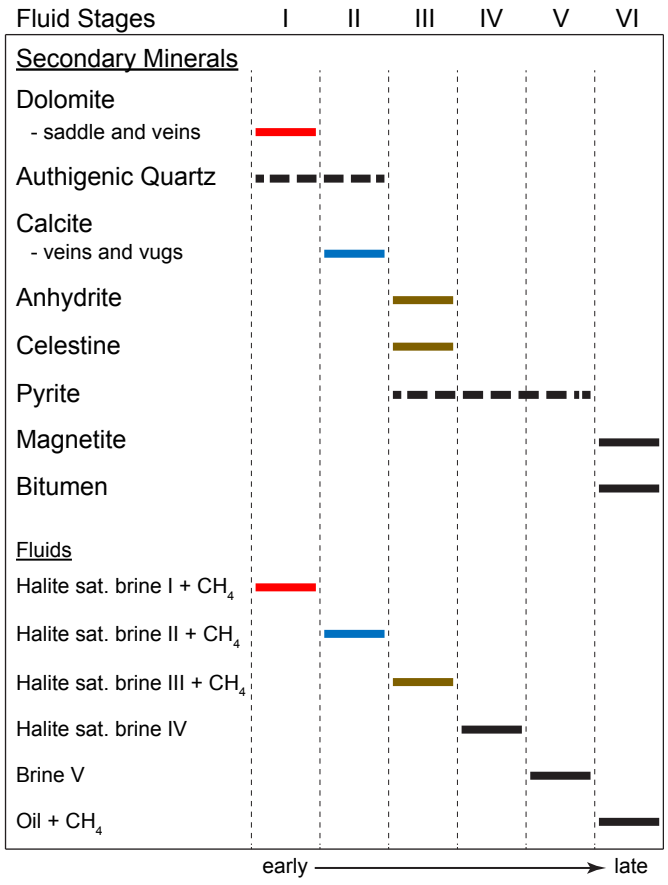

Fig. 3. Relative timing of secondary mineral formation and trapping of fluid inclusion stages I–VI, based on detailed petrography. The timing of authigenic quartz and pyrite formation relative to fluid stages I–II and III–V, respectively, is uncertain and indicated by the dashed lines. *Note*: matrix replacement dolomite predates the formation of saddle dolomite.

observed in each inclusion assemblage (Diamond et al., 2015). Uniform proportions of liquid and vapour were observed in assemblages of stage IV inclusions (e.g., Fig. 6B–C, E), thus the maximum T_h for each assemblage represents a minimum constraint on T_{trap} (i.e. $T_{trap} > T_{h,max}$). All assemblages in stages I to IV contain variable proportions of halite, indicating they were saturated with respect to halite at the time of trapping (principles of these interpretations are explained in Diamond, 2003). Stage V inclusions consist of saline brine without vapour bubbles at room temperature (e.g., Fig. 6G). In this case, the only constraint on T_{trap} is the empirical rule that they were trapped below 70 °C (Goldstein and Reynolds, 1994; Diamond, 2003). The T_{trap} results are summarized in Fig. 7 and Table 1 (detailed T_h data are shown in Table 2S – Supporting Material, after Diamond et al., 2015). The relative timing of fluid inclusion entrapment associated with stages IV vs. VI was determined by cross-cutting relationships as shown in Fig. 6H and I.

Temperatures of final melting of ice, T_m(ice), in the presence of halite + liquid + vapour were measured in assemblages of inclusions in stages I to IV. No observations of eutectic melting could be made but the span of T_m(ice) values between −52.7 and −34 °C suggests the principal salts are NaCl and $CaCl_2$. As commonly observed in $CaCl_2$-rich inclusions, nominally stable hydrohalite nucleated only rarely upon cooling and so the measured T_m(ice) transitions represent metastable equilibria. To enable salinity determinations from these data, the locus of the metastable cotectic involving ice + halite + liquid + vapour was calculated for this study (red curve Fig. 8A and B) from the stable phase relations for the H_2O–NaCl–$CaCl_2$ ternary system given by Oakes et al. (1990) and Steele-MacInnis et al. (2011). Fluid compositions and salinities in terms of the model ternary components were then obtained for each assemblage by constructing a halite-melting path beginning at T_m(ice) on the cotectic and moving towards the NaCl apex of the ternary. The point at which this path intersects T_{trap} on the halite liquidus defines the ternary composition and the salinity of the inclusions (i.e. green arrow in Fig. 8A). For the halite-undersaturated inclusions of stage V, salinity could only be broadly constrained to lie along the relevant isotherms of T_m (ice) (dark bands in Fig. 8B; question marks show range of uncertainty in salinity). Table 1 lists the resulting ternary compositions and salinities. Microthermometric data of all individual inclusions measured are given in Diamond et al. (2015) and are shown in Table 2S (Supporting Material).

Primary, stage I inclusions in saddle dolomite (e.g., Fig. 5A–C) from the Coboconk and Gull River formations yielded the highest T_{trap} values; 122–128 °C ($n = 3$) and a T_{trap} value of 88 °C was obtained for primary inclusions in rhombic dolomite from the Cambrian. Stage I inclusions have T_m (ice) values between −44.1 and −41.5 °C, implying that the fluid had a salinity of 33–34 wt% $[CaCl_2+NaCl]_{eq}$ at halite saturation (at the time of T_{trap}).

Primary stage II inclusions in calcite (e.g., Fig. 5D–F) yielded T_{trap} values between 54 and 78 °C (mean and S.D. of 65 ± 9 °C; $n = 7$) and T_m (ice) values between −47.9 and −35.9 °C. Inclusions in two Coboconk samples yielded T_m (hydrohalite) values from −22.9 to −16.5 °C. The calculated salinity of the halite-saturated stage II fluid at T_{trap} varies between 30.7 and 33.2 wt% $[CaCl_2+NaCl]_{eq}$.

Stage III is represented by primary inclusions in celestine and anhydrite (e.g., Fig. 5G–I) and by early secondary inclusions in stage II calcite. Crystallites of anhydrite were occasionally identified in stage III inclusions in calcite (Diamond et al., 2015). The inclusions in celestine and calcite yielded T_{trap} values between 42 and 80 °C and T_m (ice) values from −46.5 to −33.2 °C, corresponding to salinities of 32–33 wt% $[CaCl_2+NaCl]_{eq}$ for the halite-saturated stage III fluid at T_{trap}.

Secondary, stage IV inclusions in calcite (e.g., Fig. 6A–E) have minimum T_{trap} values between 57 and 106 °C. Their T_m (ice) values vary from −52.7 to −26.4 °C, which indicates a narrow range of halite-saturated salinities between 32 and 34 wt% $[CaCl_2+NaCl]_{eq}$ for this gas-undersaturated fluid at minimum T_{trap}.

Late secondary, liquid-only (metastable) inclusions associated with stage V (e.g., Fig. 6F and G) formed at temperatures <70 °C (Goldstein and Reynolds, 1994) and were identified in calcite and dolomite throughout the sample suite. Stage V inclusions from the Gull River Formation and the Cambrian show T_m(ice) values of −35.0 to −24.3 °C, indicating salinities of 23–26 wt% $[CaCl_2+NaCl]_{eq}$.

Hydrocarbon inclusions (stage VI) in calcite (e.g., Fig. 6H and I) from the Coboconk and Gull River formations contain variable proportions of liquid oil and methane vapour, indicating they were gas-saturated at the time of trapping. Their minimum T_h values yield T_{trap} values of 48 and 59 °C, respectively.

4.3. C- and O-isotope compositions

Calcite vein and vug samples from the Cambrian sandstones yielded the most ^{13}C-depleted C-isotope compositions in the sedimentary succession, with $\delta^{13}C$ values of −6.1 to −3.5‰ (Fig. 9A; Table 3S – Supporting Material). Cambrian dolomite samples, including one dolostone and one saddle dolomite, have $\delta^{13}C$ values of −2.5‰ and −3.8‰, respectively. Similar C-isotope compositions were obtained for two samples from a vug in the Shadow Lake

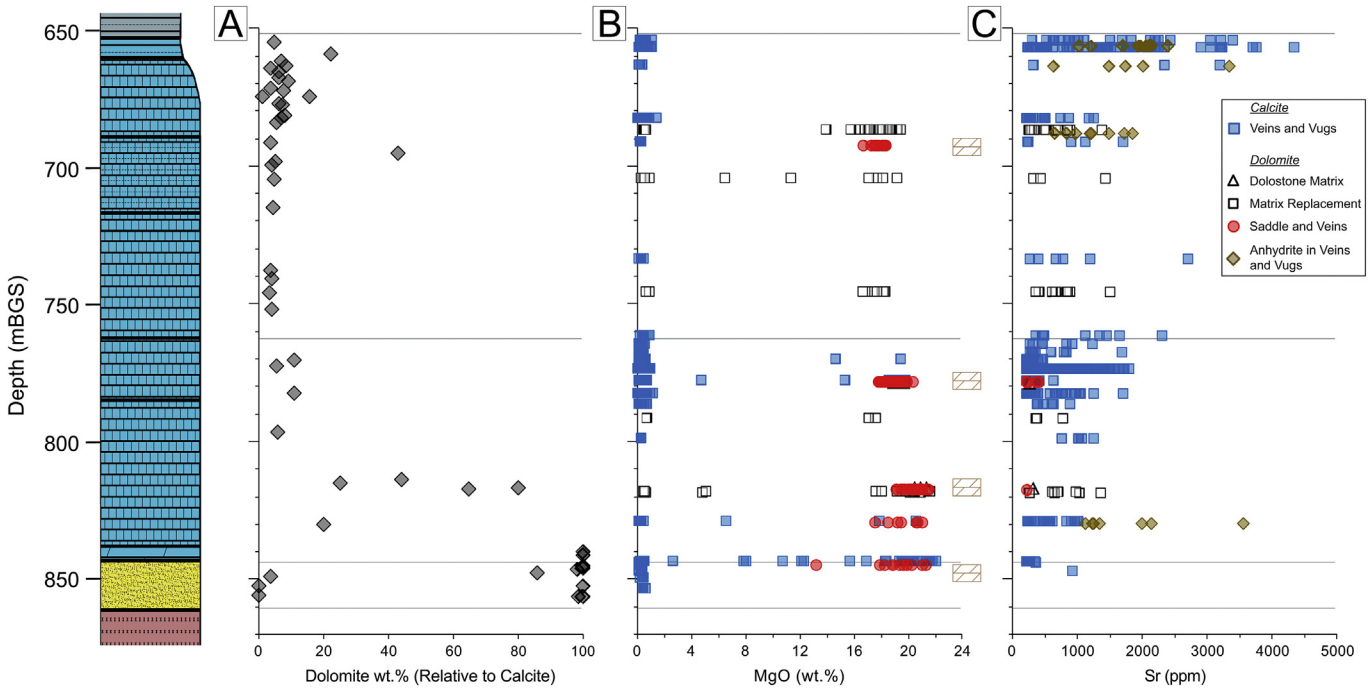

Fig. 4. Compositions of the secondary minerals in the DGR samples, including wt% dolomite relative to calcite (A), which was determined using XRD (Saso, 2013) and MgO (B) and Sr (C) concentrations determined using EPMA. Note, the location of stratabound dolostone layers in the succession are indicated in (B) by block symbols. Boundaries in the sedimentary succession are also shown here (in descending order): Queenston–Collingwood/Cobourg (Trenton Group); Kirkfield (Trenton Group)–Coboconk (Black River Group); Shadow Lake (Black River Group)–Cambrian; Cambrian–Precambrian.

Formation, including $\delta^{13}C$ values of −3.4‰ for saddle dolomite and −5.0‰ for calcite (Table 3S – Supporting Material).

A pronounced C-isotope shift of +2 to +3‰ occurs at the boundary between the Shadow Lake and Gull River formations. Uniform C-isotope compositions are observed for most samples from the base of the Gull River Formation to the Cobourg Formation, with $\delta^{13}C$ values of −1.0 to +1.9‰ and no identifiable differences between the Black River and Trenton group samples. Similarly, no differences in $\delta^{13}C$ are observed between samples of limestone matrix and calcite veins and vugs, and samples of saddle dolomite, dolostone and matrix replacement dolomite. Although most of the C-isotope data are constant versus depth, three calcite vein samples from a 3 m section at the base of the Kirkfield Formation (DGR-6-864.60; DGR-6-865.20; DGR-6-867.60) vary by 2.7‰ (−0.8 to +1.9‰; Fig. 9A). It should be noted, however, these data fall within the broader range of C-isotope compositions defined by other samples from the Ordovician succession, including a limestone from the Gull River Formation (−1.0‰) and dolostone from the Coboconk Formation (+1.9‰).

Calcite vein and vug samples from the Cambrian have $\delta^{18}O$ values between +14.6‰ and +24.2‰ and overall represent the most ^{18}O-depleted compositions in the succession, with only one of these Cambrian calcite samples higher than +17.8‰, (Fig. 9B; Table 3S – Supporting Material). Two dolomite samples from the Cambrian units have $\delta^{18}O$ values of +23.0‰ (dolostone) and +23.2‰ (saddle dolomite). Two samples from a vug in the Shadow Lake Formation (DGR-2-843.83) yielded similar O-isotope compositions to the other respective calcite and dolomite samples in the Cambrian sample suite, and include $\delta^{18}O$ values of +15.9‰ for calcite and +20.6‰ for saddle dolomite.

A pronounced shift of ~ +3 to +7‰ is observed in the $\delta^{18}O$ data along the boundary between the Shadow Lake and Gull River formations (Fig. 9B). Calcite vein and vug samples from the Gull River and Coboconk formations have a wide range of $\delta^{18}O$ values, from +18.9 to +26.7‰. Notably, a ~10 m section at the top of the Coboconk Formation, along the Trenton–Black River group boundary, exhibits a spread in $\delta^{18}O$ values of up to 5.4‰ (+21.3 to +26.7‰). Calcite veins and vug samples from the Trenton Group have $\delta^{18}O$ values from +23.0 to +28.1‰, and are broadly consistent with calcite O-isotope data for the Black River Group. Most of the Trenton Group calcite samples vary by up to 3.1‰, with only one exceptional $\delta^{18}O$ value higher than +26.1‰ (Fig. 9B). Six saddle dolomite samples from the combined Black River–Trenton group units have uniform $\delta^{18}O$ values of +20.3 to +21.3‰, and are > 1–2‰ lower in $\delta^{18}O$ than most calcite vein and vug samples in the Ordovician succession. In contrast, one sample of dolostone matrix (DGR-2-778.44) and one replacement dolomite sample (DGR-4-772.10) from the Coboconk Formation yielded $\delta^{18}O$ values of +23.6‰ and +22.0‰, respectively. Eleven limestone matrix samples from the Trenton and Black River groups exhibit a subtle trend of increasing $\delta^{18}O$ values towards the surface, from +23.8 to +26.8‰, and no identifiable shifts or sections of O-isotope variability along the boundary between the two groups, as observed in the calcite vein and vug data (Fig. 9B).

4.4. Sr-isotope ratios

Secondary calcite and dolomite samples from the Cambrian units have the highest Sr-isotope ratios in the sedimentary succession. Four calcite vein/vug samples have $^{87}Sr/^{86}Sr$ values from 0.70975 to 0.71039, while one sample of dolostone matrix and one saddle dolomite yielded similar $^{87}Sr/^{86}Sr$ values of 0.71043 and 0.71027, respectively (Fig. 9C; Table 3S – Supporting Material). Furthermore, two calcite/saddle dolomite samples from a vug in the Shadow Lake Formation have $^{87}Sr/^{86}Sr$ values of 0.71037 and 0.70984, and overlap in Sr-isotope composition with other samples from the Cambrian.

A shift in $^{87}Sr/^{86}Sr$ of up to ~ −0.02 is observed across the

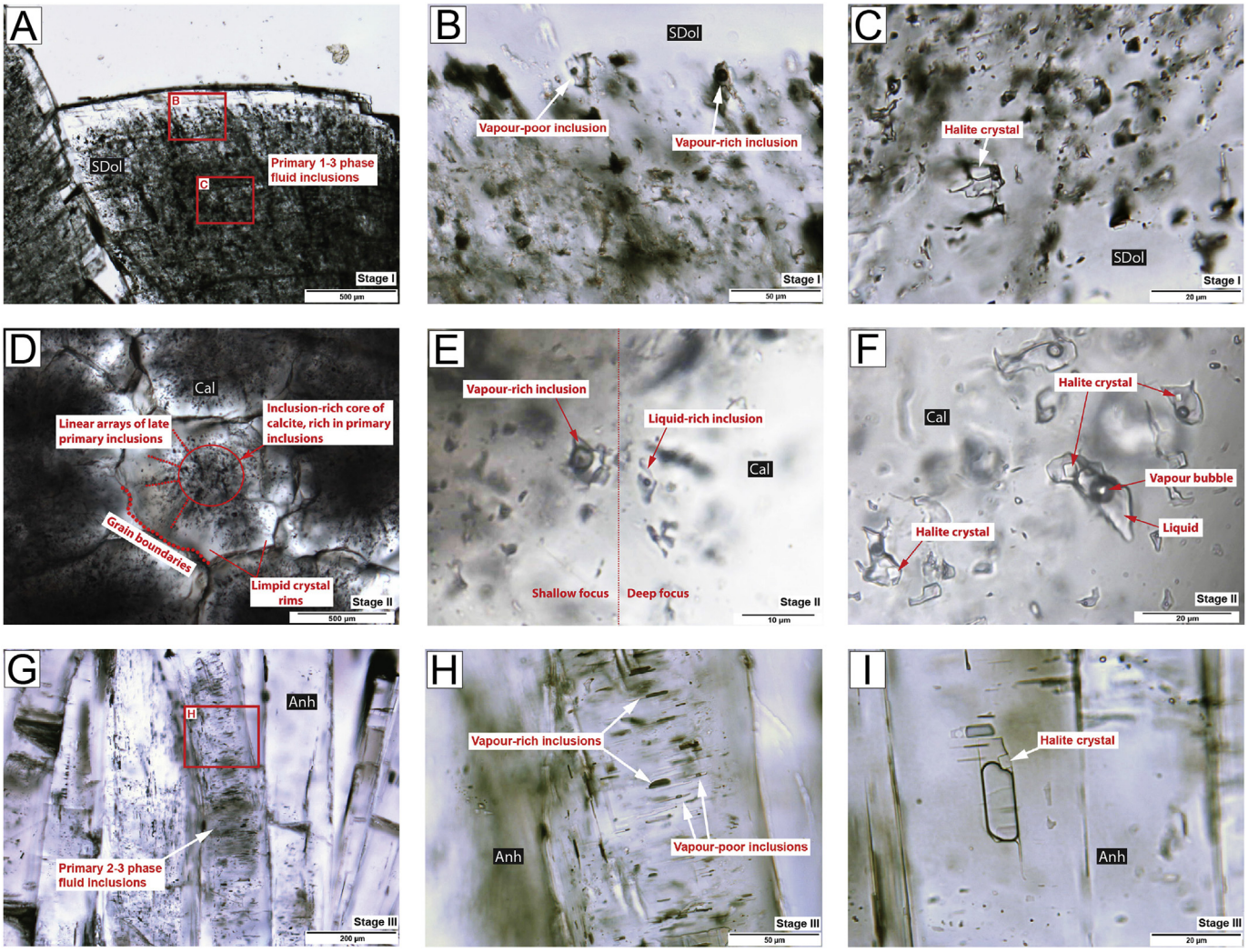

Fig. 5. Photomicrographs of fluid inclusions representative of paleofluid stages I–III, all viewed in plane-polarized, transmitted light. (A) Stage I in DGR-4-829.53, saddle dolomite crystal showing curved crystal faces lining the walls of a vug. The core is rich in primary fluid inclusions and is overgrown by a clear, inclusion-free outer rim; (B–C) Details of A showing variable proportions of liquid brine, CH_4–CO_2–vapour and halite within individual inclusions of the same assemblage, indicating that all three phases were present at mutual saturation during fluid entrapment; (D) Stage II in DGR-3-799.15, calcite crystals in a vug, containing clouds of three-dimensionally distributed primary fluid inclusions. The rims of these crystals contain linear arrays of fluid inclusions that radiate outwards, parallel to the growth direction of the crystal, and are indicative of primary inclusions. All are younger than inclusions in A, because calcite systematically overgrows saddle dolomite (Fig. 2H); (E–F) Details of D showing variable proportions of liquid brine, CH_4–vapour and halite within individual inclusions of the same assemblage, indicating that all three phases were present at mutual saturation during fluid entrapment; (G) Stage III in DGR-4-829.53, primary inclusions within fibrous anhydrite. The inclusions are younger than in D, because anhydrite systematically overgrows calcite (Fig. 2A); (H–I) Details of G showing variable proportions of liquid brine, CH_4–vapour and halite within individual inclusions of the same assemblage, indicating that all three phases were present at mutual saturation during fluid entrapment.

boundary between the Shadow Lake and the Gull River formations. Calcite vein and vug samples from the Gull River and Coboconk formations have the highest Sr-isotope variability in the succession, with $^{87}Sr/^{86}Sr$ values ranging from 0.70799 to 0.70990 (Fig. 9C). Similar variability is observed for three samples of saddle dolomite, one dolostone and one sample of anhydrite from the Gull River–Coboconk units, with combined $^{87}Sr/^{86}Sr$ values from 0.70854 to 0.70939. In contrast, three limestone samples from these Black River Group units (two Gull River, one Coboconk) have uniform $^{87}Sr/^{86}Sr$ values of 0.70810–0.70833, and overlap with the lowest Sr-isotope ratios of calcite veins from these units.

For the Trenton Group, five calcite vein/vug samples and three limestone matrix samples have uniform $^{87}Sr/^{86}Sr$ values of 0.70790–0.70817 (Fig. 9C), and are consistent with the $^{87}Sr/^{86}Sr$ values of limestone samples from the underlying Black River Group. Similar $^{87}Sr/^{86}Sr$ values of 0.70818, 0.70808 and 0.70848 are observed for anhydrite samples from the Cobourg and Sherman Fall formations, and a celestine sample from the Kirkfield Formation, respectively (Fig. 9C). One sample of saddle dolomite from a vug in the Sherman Fall Formation (DGR-5-743.10) has an exceptional $^{87}Sr/^{86}Sr$ value of 0.70856. However, this sample has an associated 2σ analytical uncertainty of ±0.00083, which is 20–40 times larger than other analyses (Table 3S – Supporting Material).

5. Discussion

5.1. Paragenetic sequence

Overall six distinct fluid events were identified in the microthermometric/petrographic results (Figs. 3 and 7), with the first two stages responsible for most of the mineral precipitation in veins and vugs and only minor amounts of anhydrite and celestine

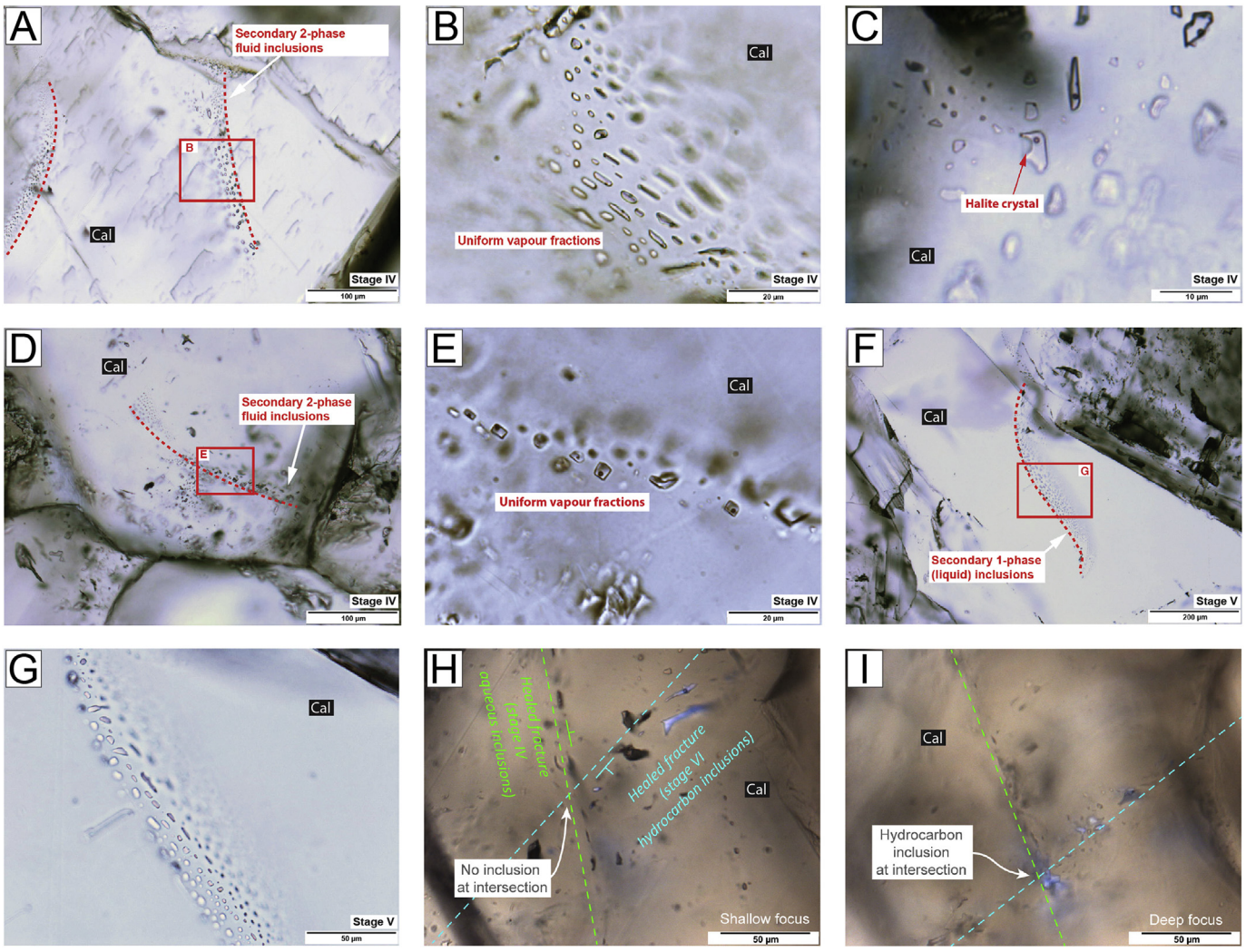

Fig. 6. Photomicrographs of fluid inclusions representative of paleofluid stages IV–VI, all viewed in plane-polarized, transmitted light. (A) Stage IV in DGR-2-847.42, planar array of secondary fluid inclusions on a healed fracture in vein calcite; (B–C) Details of A showing uniform proportions of liquid brine and H_2O–vapour but variable proportions of halite within individual inclusions of the same assemblage. The inclusions homogenize to liquid, therefore only brine and halite were present (without free vapour) at mutual saturation during fluid entrapment; (D) Stage IV in DGR-2-691.70, planar array of secondary inclusions on a healed fracture in vein calcite, as in A; (E) Detail of D showing the same relations as in (B). This key assemblage homogenizes to liquid at 106 °C; Sample (F) Stage V in DGR-2-844.31, planar array of secondary liquid-only inclusions (metastable stretched water) on a healed fracture in vein calcite. Such assemblages cross-cut stage IV assemblages (not shown); (H) Stages IV and VI in DGR-6-892.99, viewed in simultaneous transmitted and UV epi-illumination. Interpretation of relative timing of secondary fluid inclusion generations based on cross-cutting relations. Traces of two healed fractures are visible, each marked by secondary fluid inclusions. *Green:* Stage IV aqueous inclusions within a fracture trace that strikes to top-left of image and dips steeply to top-right. *Blue:* Stage VI blue fluorescent liquid hydrocarbon inclusions with CH_4-vapour bubbles in a fracture trace that strikes to top-right and dips shallowly to bottom-right. No inclusion is present at the intersection of the fracture traces (at shallow focus), so the relative ages of the two fractures are ambiguous; (I) Same view as H but at a deeper focus level. A hydrocarbon inclusion is present at the intersection of the fracture traces, indicating that the hydrocarbon inclusions and their host fracture are younger than the aqueous inclusions and their corresponding host fracture. (For interpretation of the references to colour in this figure legend, the reader is referred to the web version of this article.)

that formed during stage III. Based on the preservation of well-defined dolomite, calcite, anhydrite and celestine crystal margins from precipitation events during stages I to III (Fig. 2), and on the absence of dissolution features, fluid stages IV–VI are interpreted as migration of relatively minor quantities of fluids along grain boundaries or micro-fractures.

Stage I is represented by formation of Fe- and Mn-enriched saddle dolomite in the Black River Group (Diamond et al., 2015) that resulted from the influx of a halite-saturated brine (34 wt% $[CaCl_2+NaCl]_{eq}$) and free methane gas at temperatures of 122–128 °C. Elsewhere in the Michigan Basin, high temperatures have been determined for fluid inclusions in saddle dolomite from the Trenton–Black River groups, including up to ~160 °C in the Albion-Scipio oil field of south-central Michigan (Allan and Wiggins, 1993) and temperatures as high as ~170 °C and 220 °C in dolomite samples from Manitoulin Island and southwestern Ontario, respectively (Coniglio et al., 1994). Elevated temperatures of ~97–144 °C were also obtained by Haeri-Ardakani et al. (2013) for saddle dolomite samples from the Trenton Group in southwestern Ontario. Davies and Smith (2006) suggested that the formation of saddle dolomite in these fault-controlled reservoirs is due to ascending fluid that is hotter than the ambient or burial temperatures of the host formation (i.e. hydrothermal). In our study, a third Fe- and Mn-enriched saddle dolomite sample from the Cambrian yielded a significantly lower T_{trap} value of 88 °C, but a similarly high salinity of 34 wt% $[CaCl_2+NaCl]_{eq}$. It is not known whether these saddle dolomite samples are contemporaneous.

Stage II primary inclusions in calcite have T_{trap} values of 54–78 °C (mean 65 ± 9 °C; $n = 7$) and represent a halite-saturated brine with a salinity of 31–37 wt% $[CaCl_2+NaCl]_{eq}$ and entrained

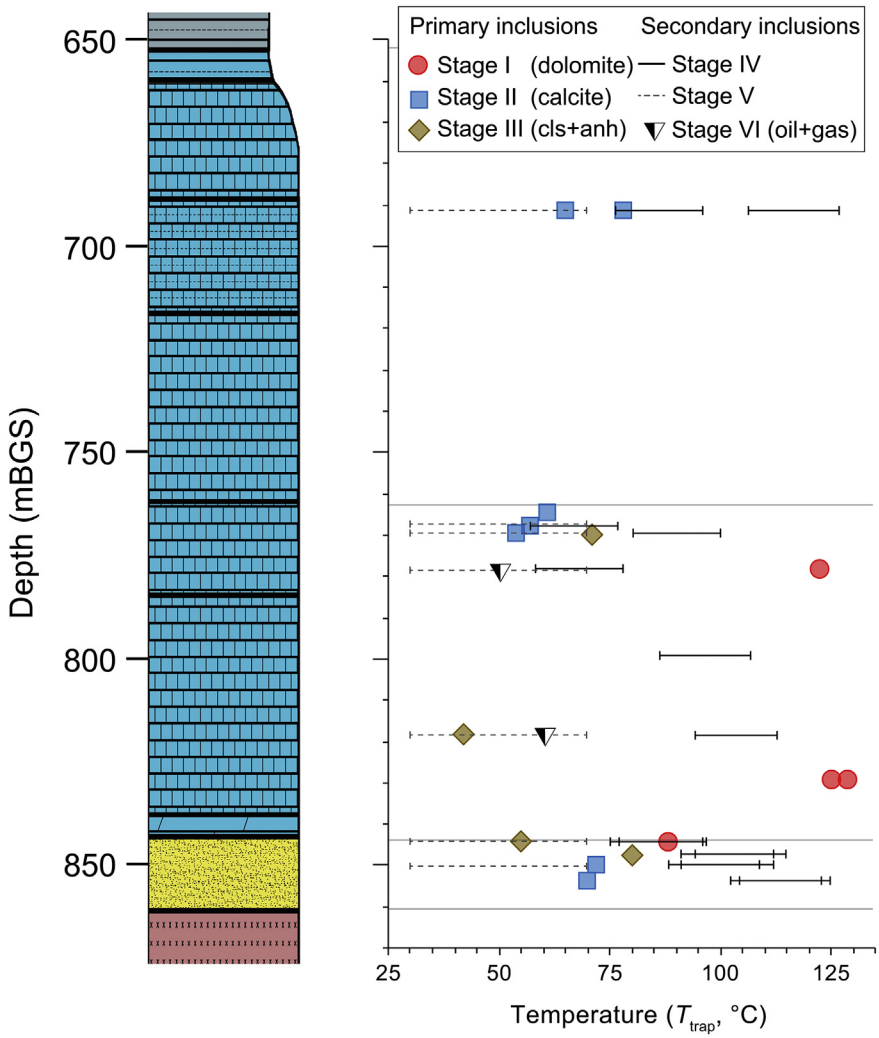

Fig. 7. Microthermometric data for assemblages of primary and secondary fluid inclusions in the secondary minerals. For the stage IV inclusions, which have uniform liquid–vapour proportions, each symbol represents a range of estimated temperatures between the minimum T_{trap} value (i.e. $T_{h,max}$) and a pressure corrected T_{trap} value, which was calculated for peak burial conditions using an estimated burial depth of 1860 m (see section 5.1). Estimated T_{trap} values of 30–70 °C are indicated for stage V inclusions. Boundaries in the sedimentary succession are also shown here (in descending order): Queenston–Collingwood/Cobourg (Trenton Group); Kirkfield (Trenton Group)–Coboconk (Black River Group); Shadow Lake (Black River Group)–Cambrian; Cambrian–Precambrian.

free methane gas. Based on the predominance of calcite as a vein/vug mineral, it can be presumed that stage II was the most significant vein- and vug-forming fluid event. The range of T_{trap} values from stage II inclusions is slightly lower than minimum paleotemperature estimates of 80 °C at the base of the Silurian and 90 °C at the base of the Trenton Group reported by Legall et al. (1981). Determinations of the absolute timing of vein and vug calcite formation in the Trenton–Black River groups have been made using U-Pb dating methods with laser ablation inductively coupled plasma mass spectrometry (LA-ICP-MS) and TIMS (Davis, 2013). Davis (2013, 2017) reported a LA-ICP-MS U-Pb age of 434 ± 5 Ma, based on a calculated mean of three model age determinations from the Cobourg and Coboconk formations, and a TIMS U-Pb date of 451 ± 38 Ma for a calcite vein from the Cobourg Formation. The Davis (2013, 2017) U-Pb data compare well with a Rb-Sr isochron age of 425 ± 6 Ma (errorchron age of 440 ± 50 Ma) by Harper et al. (1995) and 7 combined K-Ar dates ranging from 453 ± 9 Ma to 412 ± 8 Ma by Harper et al. (1995) and Ziegler and Longstaffe (2000) (weighted mean of 442 ± 16 Ma) for secondary K-feldspar obtained along the Precambrian–Paleozoic boundary in southern Ontario. These data suggest the influx of stage II, calcite-forming fluids in the Trenton–Black River groups likely occurred between the Late Ordovician and Silurian.

Stage III fluid inclusions have T_{trap} values of 42–80 °C and represent a stage of fluid migration during which anhydrite and celestine were formed. The mean T_{trap} value of 62 ± 17 °C for four stage III inclusions is similar to the mean T_{trap} value (65 ± 9 °C; $n = 7$) for stage II primary inclusions in calcite. Salinities of stage III inclusions range from 32 to 33 wt% $[CaCl_2+NaCl]_{eq}$, and are comparable to the salinity estimates for stage I and stage II inclusions. This suggests a paragenetic link between the stage I–III fluids, with saddle dolomite forming during initial brine influx at 122–128 °C (stage I), then subsequent cooling and formation of calcite (stage II) and penecontemporaneous formation of anhydrite and celestine (stage III).

Secondary fluid inclusions defining stage IV have minimum T_{trap} values between 57 and 106 °C, including one calcite vein from the Sherman Fall Formation (DGR-2-691.70; see Fig. 6D and E) that yielded minimum T_{trap} values ranging from 77 to 106 °C. The absolute timing and burial depth (i.e. thickness of overburden sediments) at the time of stage IV fluid inclusion entrapment is unclear, therefore, definitive pressure corrections to determine T_{trap} (true)

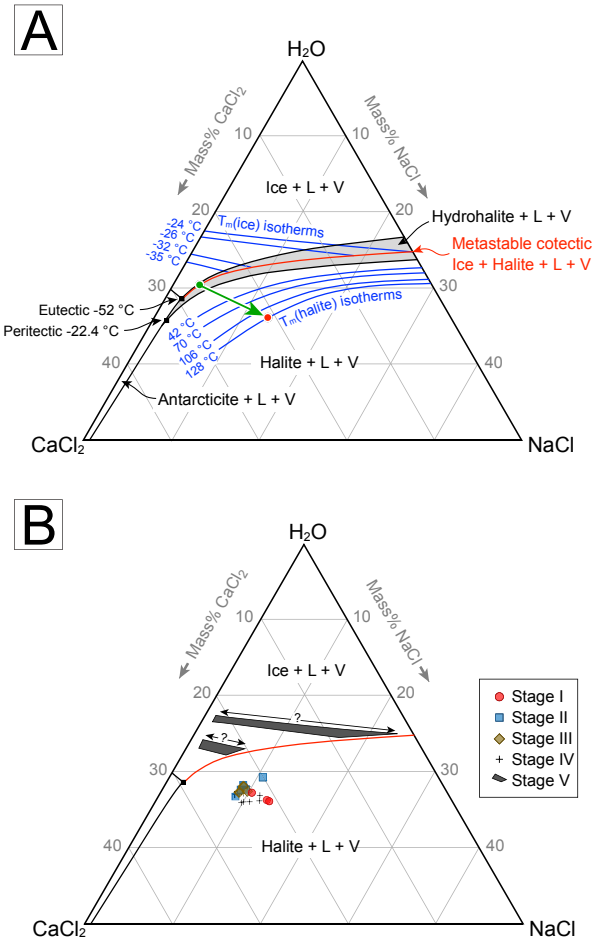

Fig. 8. Salinity estimates for assemblages of primary and secondary fluid inclusions in the secondary minerals, derived from T_m (ice) values for all fluid stages (A–B) shown in a H_2O–NaCl–$CaCl_2$ ternary model. Stable phase relations of Oakes et al. (1990) and Steele-MacInnis et al. (2011) are also shown in (A). The metastable cotectic in (A) and (B) was calculated in this study.

cannot be applied to the stage IV data. In order to determine an upper limit for stage IV fluid inclusion entrapment, T_{trap} (maximum) values were calculated using pressure corrected data for peak burial conditions for the Ordovician–Cambrian succession. This is a conservative approach because we do not know that stage IV coincides with peak burial, and because all corrections are made to the depth at the base of the Paleozoic succession. After peak burial conditions, it can be inferred from the work of Coniglio and Williams-Jones (1992) that approximately 1000 m of Paleozoic sediments were eroded from the sedimentary succession at the Bruce site (NWMO, 2011). Utilizing an overburden thickness of 1000 m and a current depth of 860 m for the base of the Paleozoic succession, a maximum burial depth of 1860 m was used to calculate an upper limit for stage IV fluid inclusion entrapment. Pressure corrected T_{trap} (maximum) values for the stage IV inclusions range from 77 to 127 °C (Fig. 7; Table 1).

There are two models that explain the formation of stage IV fluids: (1) influx of hydrothermal brines, or (2) regional heating of the sediments (i.e. through conduction), coupled with fracturing and re-mobilization of fluids. For model 1, significant quantities of fluid and high flow rates along permeable structures would be required to facilitate the transfer of heat, but there is no evidence for fluid movement at this scale (e.g., large fracture/vein systems, dissolution/re-precipitation features, formation of new secondary minerals with primary inclusions analogous to stage IV). Alternatively, a regional heating event (model 2) is consistent with an estimated minimum paleotemperature of 90 °C at the base of the Trenton Group (Legall et al., 1981). Evidence for a regional heating event exists elsewhere in the Michigan Basin. Temperatures of ~70–170 °C and ~40–260 °C have been obtained for secondary fluid inclusions in calcite from Trenton–Black River rocks on Manitoulin Island and in southwestern Ontario, respectively (Coniglio et al., 1994). Haeri-Ardakani et al. (2013) also reported temperatures of ~60–131 °C for fluid inclusions in calcite cement samples from the Trenton Group in southwest Ontario. In central Michigan, fluid inclusions in Middle Ordovician St. Peter Formation sandstones yielded temperatures of 76–169 °C for quartz overgrowths, and 94–149 °C for dolomite cements (Girard and Barnes, 1995), and are consistent with temperatures of ~100–160 °C obtained for fluid inclusions in saddle dolomite from elsewhere in central Michigan (Allan and Wiggins, 1993). Overall, these high temperatures (up to 260 °C) strongly suggest that regional heat sources were present at depth below the Michigan Basin. Reactivation of the mid-continent rift was suggested by Ma et al. (2009) as a source of heat and mantle-derived He and Ne anomalies in the hydrothermal fluids that interacted with the basin rocks. Regional-scale heating has also been linked to the formation of secondary illite at 367–322 Ma in the St. Peter sandstone along the base of the Paleozoic succession (Girard and Barnes, 1995). Reactivation of the mid-continent rift during the Late Devonian–Mississippian could be responsible for initiating regional-scale heating below the Michigan Basin and may be linked to the stage IV fluid migration event observed in the Ordovician carbonates at the Bruce site.

Stage V and VI inclusions represent the latest observed records of fluid migration in the sedimentary succession, and for the latter stage VI fluids, include hydrocarbon inclusions in the Coboconk and Gull River formations and the Cambrian units. Samples from the Coboconk and Gull River formations yielded trapping temperatures of 48 and 59 °C (Fig. 7). The occurrence of hydrocarbon fluids is consistent with the presence of bitumen layering or oil in the Coboconk, Gull River and Shadow Lake formations (see Fig. 2.32 in Intera, 2011), suggesting that stage VI represents an important period of hydrocarbon generation and/or migration in the Black River Group.

5.2. Source and evolution of fluids

By combining the petrographic and fluid inclusion results with the C- O- and Sr-isotope data, inferences can be made about the sources and paleofluid evolution through the secondary-mineral formation events of stages I to III. Secondary calcite (veins/vugs) and dolomite (dolostone matrix and saddle) samples from the combined Cambrian–Shadow Lake units have $\delta^{13}C$ values of ~ −6.1 to −2.5‰ (Fig. 9A). Estimates of the average C-isotope composition of Cambrian seawater include $\delta^{13}C$ values between −0.9‰ and +0.0‰ (Fig. 9A; Veizer et al., 1999), suggesting that the calcite and dolomite samples from the Cambrian–Shadow Lake units were not sourced from connate fluids derived from Cambrian seawater. Alternatively, these low $\delta^{13}C$ values reflect carbonate mineral formation from fluids that reacted with organic carbon. Harper et al. (1995) reported similar ^{13}C-depleted data (−9.3 to −3.9‰) for secondary calcite and dolomite associated with hydrothermally altered granitoid rocks along the Precambrian–Paleozoic boundary in southern Ontario.

A 2–3‰ shift in $\delta^{13}C$ occurs at the boundary between Cambrian–Shadow Lake units and the overlying Gull River Formation. The C-isotope compositions of calcite and dolomite samples show little scatter through the Gull River to Cobourg formations (Fig. 9A)

Table 1
Microthermometric results for fluid inclusions in the secondary minerals.

Sample ID	Formation	mBGS	Matrix	Mineral	T_{trap} (°C)						T_m(ice) or T_m(hydrohalite)[d] (°C)									
					I	II	III	IV[b]	V	VI	I		II		III		IV		V[c]	
											min	*max*	*min*	*max*	*min*	*max*	*min*	*max*	*min*	*max*
DGR-2-691.70	Sherman Fall	691.70	cal-py	cal		65 78		[77–96] [106–127]	<70				−46.9	−40.9			−45.2	−44.7		
DGR-6-883.75	Coboconk	764.65	dol	cal		61							*−21.5*	*−18.2*	−36.4	−33.2	−40.7	−39.0		
DGR-6-886.91	Coboconk	767.81	dol	cal		57		[57–77]	<70						−45.0	−34.0	−47.0	−42.0		
DGR-4-769.57	Coboconk	769.57	cal-py	cal-cls		54	71	[80–100]	<70				−44.2	−35.9	−46.5	−35.2				
DGR-6-892.99	Coboconk	778.29	dol	cal				[61–78]	<70	48							−46.8	−42.1		
DGR-2-778.44	Coboconk	778.44	dol-py	dol (SD)	122[a]															
DGR-3-799.15	Coboconk	799.15	cal	cal				[86–107]					*−22.9*	*−18.4*						
DGR-4-818.36	Gull River	818.36	dol-py	cal			42	[94–113]	<70	59			−43.1	−40.2			−38.8	−44.1		
DGR-4-829.53	Gull River	829.53	dol-py	dol (SD)	125 128[a]						−44.1	−42.7								
DGR-2-844.31	Cambrian	844.31	dol-py	dol-cal	88[a]		55	[75–96] [77–97]	<70		−42.7	−41.5			−40.3	−37.4	−43.9	−42.6	−35.0	−34.4
DGR-2-847.42	Cambrian	847.42	qtz	cal			80	[91–112] [94–115]							−42.9	−41.8	−52.1	−50.5		
DGR-2-850.01	Cambrian	850.01	qtz	cal		72		[88–109] [91–112]	<70				−42.6	−41.5			−52.1	−49.5	−34.2	−32.1
DGR-2-853.72	Cambrian	853.72	qtz	cal		70		[102–123] [104–125]	<70				−47.9	−42.6			−52.7	−50.3	−25.9	−24.3

Notes: Microthermometric measurements were made in calcite and dolomite ([a]), and are indicated by the Mineral column. Relative timing of fluid stages I–VI was determined petrographically based cross-cutting relationships between fluid inclusion assemblages. ([b]) T_{trap} for stage IV can only be bracketed between T_h (minimum possible value) and a maximum T calculated from an assumed lithostatic pressure of 1860 m (see text for explanation). T_m(ice) values in stages I–IV represent the metastable equilibrium between halite + ice + liquid + vapour. ([c]) T_m(ice) for stage V was obtained by artificially stretching the inclusions. ([d]) Hydrohalite T_m values are shown in italics. Abbreviations: cal – calcite; cls – celestine; dol – dolomite; py – pyrite; SD – saddle dolomite; qtz – quartz.

and are consistent with estimates by Veizer et al. (1999) for the average C-isotope composition of seawater during the Late Ordovician (−0.1 to +1.7‰), suggesting a C source dominated by seawater-derived connate fluids or external fluids that experienced high degrees of fluid–rock interaction with the host limestones (Fig. 9A).

Calcite samples from the Shadow Lake and Cambrian units generally have the lowest $\delta^{18}O$ values (+14.6 to +24.2‰), with most calcite veins and vugs plotting at ~ +16‰ (7 of 8 calcite veins form a calculated mean of +15.9 ± 1.0‰; S.D.). A prominent feature of the O-isotope data through the Cambrian–Ordovician succession is the >4‰ shift that occurs along the boundary between the Cambrian–Shadow Lake units and the overlying Gull River Formation (Fig. 9B). Relatively high variability is observed in the $\delta^{18}O$ data for the Coboconk Formation just below the Trenton–Black River group boundary (Fig. 9B), with values from calcite vein and vug samples exhibiting a spread of up to 5.4‰. This variability could be explained by: (1) mixing between two or more fluids that had distinct O-isotope compositions (i.e. connate vs. external hydrothermal fluids), or (2) temperature-related differences in $\Delta^{18}O_{calcite-fluid}$ during the precipitation of calcite (e.g., Friedman and O'Neil, 1977). The fact that large temperature differences are not observed in the primary fluid inclusion data for the Coboconk Formation (Fig. 7) suggests that the $\delta^{18}O$ variability may be explained by mixing with external fluids. The Trenton–Black River boundary represents a significant change in hydraulic conductivity, with rocks in the Trenton Group having K_h values up to six orders of magnitude lower than those of the Black River Group (Normani and Sykes, 2012; Beauheim et al., 2014; Khader and Novakowski, 2014). Furthermore, thin dolostone units (<20 cm) and a bentonite unit (<10 cm thick) occur as stratabound layers in the Coboconk Formation (~790.50 m and 781.00 mBGS, respectively). These units, particularly the dolostone, may have relatively high permeability and porosity compared to the bounding limestones, and as such, could represent pathways of enhanced lateral flow, allowing for ingress of external fluids.

The O-isotope compositions of source fluids responsible for secondary mineral formation were estimated using the microthermometric data and mineral–fluid O-isotope exchange thermometers for calcite (Friedman and O'Neil, 1977, Fig. 10A) and dolomite (Horita, 2014, Fig. 10B). The O-isotope composition of Late Ordovician seawater is shown in Fig. 10, with $\delta^{18}O$ values between −4 and −2‰ (Veizer et al., 1999; Shields et al., 2003). Calculated values for the O-isotope composition of fluids in equilibrium with all limestones from the Gull River to Cobourg formations are consistent with Ordovician seawater (Fig. 10A), indicating that there has been limited diagenetic or hydrothermal alteration effects to their primary O-isotope compositions.

Calcite vein and vug samples from the Cambrian–Shadow Lake units have calculated $\delta^{18}O_{fluid}$ values between ~ −6‰ and +4‰, based on formation temperatures of 70–72 °C (Fig. 10A). Gull River and Coboconk samples have similar calculated $\delta^{18}O_{fluid}$ values of ~ −6 to +4‰, while samples from the Trenton Group have calculated fluid compositions of ~ +2 to +8‰ (Fig. 10A). These fluid compositions are suggestive of calcite precipitation from Late Ordovician seawater or an ^{18}O-enriched, seawater-derived basin fluid. Similar ^{18}O-enrichments relative to seawater have been described for fluids in many sedimentary basins (Holser, 1979; Knauth and Beeunas, 1986; Ayalon and Longstaffe, 1988; Kyser and Kerrich, 1990; Wilson and Long, 1993a, 1993b; Hanor, 2001), and are interpreted to have undergone ^{18}O-enrichment by evaporation and/or fluid–rock interaction following burial. Modification

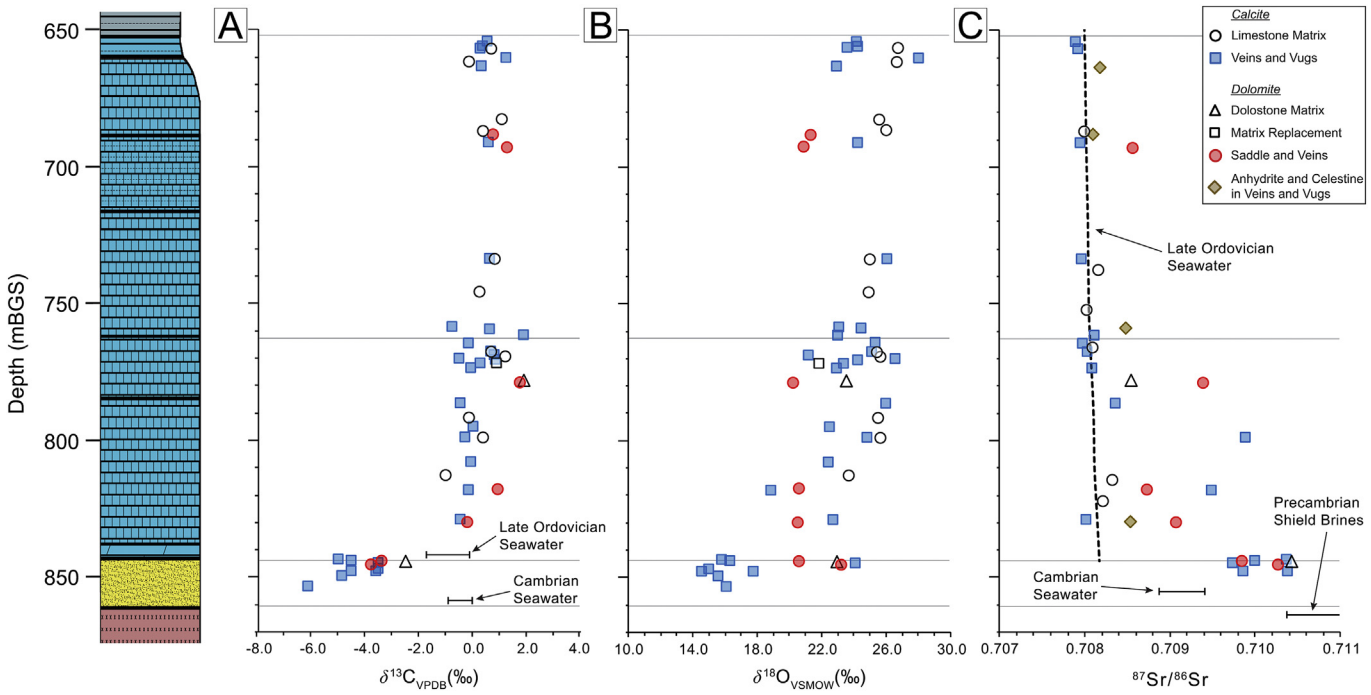

Fig. 9. C-, O- and Sr-isotope results for the secondary minerals in the Ordovician–Cambrian sedimentary succession (A–C, respectively). Average C-isotope compositions of seawater during the Late Ordovician (−0.1 to +1.7‰) and the Cambrian (−0.9 to +0.0‰) are also shown in (A) and are based on marine carbonate rocks from Veizer et al. (1999). Average $^{87}Sr/^{86}Sr$ values for Late Ordovician seawater (0.70887–0.70941) were obtained from Veizer et al. (1999). The $^{87}Sr/^{86}Sr$ values of Precambrian shield brines from the Sudbury region (0.71037–0.74009) were reported by McNutt et al. (1984). Boundaries in the sedimentary succession are also shown here (in descending order): Queenston–Collingwood/Cobourg (Trenton Group); Kirkfield (Trenton Group)–Coboconk (Black River Group); Shadow Lake (Black River Group)–Cambrian; Cambrian–Precambrian.

of seawater-derived connate fluids by influx of hydrothermal fluids that interacted with, or were derived from the Precambrian shield (Spencer, 1987) could also explain such ^{18}O-enrichments.

Calculated fluid compositions for saddle dolomite have $\delta^{18}O_{fluid}$ values of ~0 to +7‰ (Fig. 10B) and overlap with the calculated fluid compositions of calcite, suggesting that dolomite precipitated from ^{18}O-enriched hydrothermal fluids originating from evolved seawater. No microthermometry data could be obtained from fluid inclusions in samples of matrix replacement dolomite and dolostone. However, if the matrix replacement dolomite and dolostone samples formed at temperatures similar to those of calcite veins and vugs (54–78 °C) or saddle dolomite (88–128 °C), the calculated fluid compositions would be −6 to +1‰ or +1 to +7‰, respectively (Fig. 10B). These calculated fluid compositions are suggestive of matrix replacement dolomite and dolostone formation directly from Late Ordovician seawater or hydrothermal fluids derived from evolved seawater, and are broadly consistent with fluid source determinations for all other secondary minerals.

Sr-isotope data for many of the samples from the Black River Group, and all samples from the Cambrian, exhibit $^{87}Sr/^{86}Sr$ enrichment well above the seawater curve of Veizer et al. (1999). Enriched $^{87}Sr/^{86}Sr$ values (>0.710) are a common signature of Precambrian brines (e.g., Frape et al., 1984; McNutt et al., 1984; Bottomley et al., 1999), and the observed enrichment suggests vein and vug formation from shield-derived hydrothermal fluids, and/or fluid–rock interaction with shield-derived detrital minerals in the Cambrian sandstones. In contrast, all vein and vug samples from the Trenton Group, and approximately half of the samples from the Black River Group, overlap with the seawater curve of Veizer et al. (1999), suggesting they formed from either connate fluids derived from Late Ordovician seawater and/or external hydrothermal brines that underwent high degrees of fluid–rock interaction and associated modification of their original isotopic signature during transit through the underlying stratigraphy.

The combined microthermometry and isotopic data are consistent with a model of secondary mineral formation by fluid mixing; with one end member being either a shield-derived hydrothermal fluid, and/or a fluid that was isotopically influenced by detrital minerals in the Cambrian sandstone, and the second end member being a connate pore fluid derived from the Paleozoic carbonates.

5.3. *Implications for the migration of high-temperature fluids in the Ordovician limestones*

An important feature of our fluid influx model for the Ordovician sedimentary succession is the formation of dolomite in the Black River Group at temperatures of 122–128 °C, which are higher than the nearest available estimate of peak burial temperature, 55–90 °C from Coniglio and Williams-Jones (1992) at Manitoulin Island, providing evidence for migration of hydrothermal fluid.

Hydrothermal dolomite is an important reservoir for oil and gas plays within the Trenton–Black River groups in the Albion-Scipio/Stoney Point fields in south-central Michigan (Hurley and Budros, 1990; Allan and Wiggins, 1993; Davies and Smith, 2006), the Lima-Indiana field in Ohio/Indiana (Wickstrom et al., 1992) and southern Ontario (Powell et al., 1984; Middleton et al., 1993; Coniglio et al., 1994; Obermajer et al., 1999). In these regions, hydrothermal dolomite developed along large-scale extensional faults as a result of high-temperature fluid–rock interaction (up to ~ 260 °C; Coniglio et al., 1994) between limestone and hydrothermal fluids that migrated upward from the underlying Cambrian aquifer. Hydrothermal dolomite reservoirs are recognized in 2D seismic data aligned with vertical “sag” or “flower” structures, often 10s of kilometers in strike length and 100s of meters in width (e.g., Davies and Smith, 2006). At that scale, these structures represent

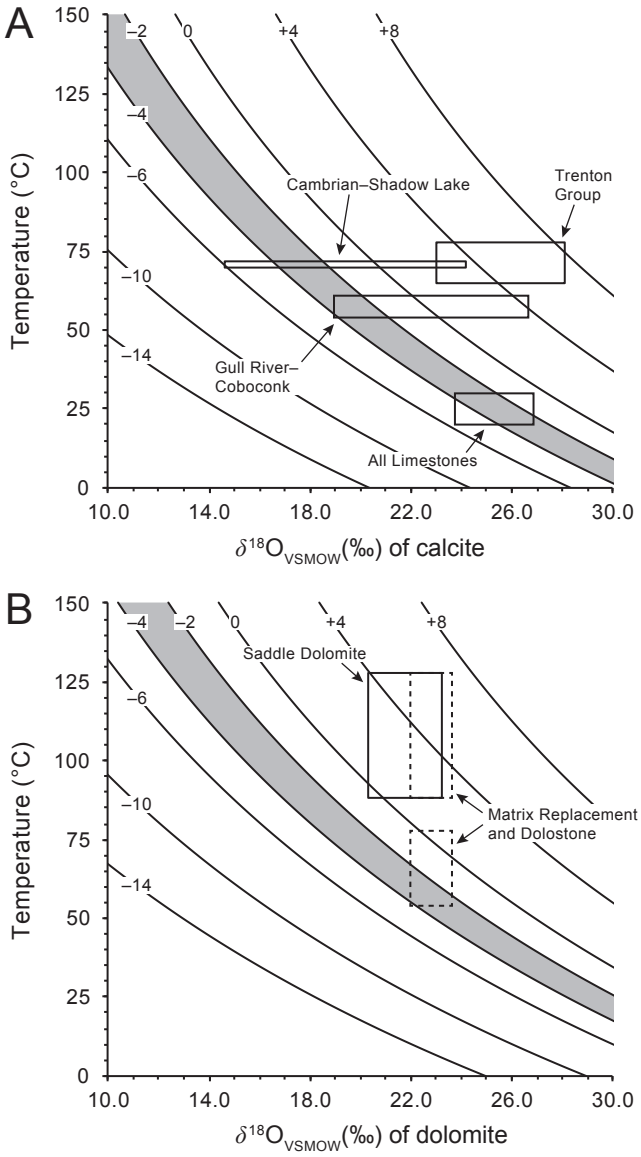

Fig. 10. Estimates of O-isotope compositions of fluids (contours) that precipitated carbonate minerals based on mineral–fluid exchange thermometers of Friedman and O'Neil (1977) for calcite (A) and Horita (2014) for dolomite (B). The boxed fields represent formation temperature estimates, based largely on fluid inclusion data discussed in Section 5.1, plotted against $\delta^{18}O$ values for each calcite/dolomite type. Formation temperatures of limestone matrix samples were estimated at 20–30 °C based on Shields et al. (2003). Cambrian–Shadow Lake calcite samples are plotted at 70–72 °C and are based on T_{trap} values for stage II fluid inclusions in these units (see Section 5.2; Table 3S – Supporting Material). Calcite vein and vug samples from the Gull River–Coboconk formations and the Trenton Group are plotted using T_{trap} temperatures of 54–61 °C and 65–78 °C, respectively. For saddle and vein dolomite, T_{trap} temperatures of 88–128 °C were used. No fluid inclusion data were obtained for dolostone and replacement dolomite samples but fluid estimates at 54–78 °C (based on calcite veins/vugs) and 88–128 °C (based on saddle dolomite) are shown by dashed boxes. The O-isotope composition of late-Ordovician seawater is indicated by the shaded bands between −2 and −4‰ (Shields et al., 2003).

regionally extensive zones of dolomitization. At the Bruce site, however, the abundance and scale of hydrothermal dolomite occurrence is much different. Saddle dolomite with associated high fluid trapping temperatures was observed in veins within Ordovician limestone, stratabound dolostone in the Ordovician, and in Cambrian dolostone. These features are typically mm or cm in thickness (e.g., Fig. 2B–E, G, H; Fig. 1S – Supporting Material), and as such, do not represent reservoir-scale structures of dolomitization as observed elsewhere in the Michigan Basin.

5.4. Conceptual model

Models for the source and timing of paleofluid movements in the Cambrian and Ordovician sedimentary units below the Bruce site, until now, have been largely based on direct geochemical and isotopic constraints from porewater extracted from drill cores (Clark et al., 2010a, 2010b; 2013, 2015; Al et al., 2015). In a detailed study, Clark et al. (2013) reported O- and H-isotope compositions and Cl- and Br-concentration data for porewater obtained throughout the Paleozoic sedimentary succession. Downward trends of decreasing Cl^- and Br^- concentrations, coupled with decreases in $\delta^{18}O$, were observed in the Ordovician limestones (Fig. 2 in Clark et al., 2013). These trends were interpreted to represent a mixing profile between hypersaline evaporated seawater from the overlying Silurian Salina Formation and shield-derived fluids (Clark et al., 2013; Al et al., 2015). The influence of a shield end member is supported by a downward trend of ^2H-enrichment – a common feature of shield fluids (Fritz and Frape, 1982; Frape et al., 1984; Pearson, 1987; Bottomley et al., 1999, 2004; Douglas et al., 2000; Gascoyne, 2004; Al et al., 2015).

Clark et al. (2013) also reported He-isotope ratios for porewater from the Ordovician shales and the Trenton and Black River group limestones. Porewater extracted from the shales and the Cobourg Formation limestone yielded uniform R/R_A values (0.020 ± 0.002; where $R/R_A = (^3He/^4He)_{sample}/(^3He/^4He)_{air}$, and $(^3He/^4He)_{air} = 1.38 \times 10^{-6}$), which are consistent with an authigenic origin, and the total He concentrations indicated a minimum period of 260 Ma for He ingrowth. A positive shift in R/R_A values was observed from the base of the Cobourg to the upper portion of the Sherman Fall Formation, followed by uniform R/R_A values of 0.035 ± 0.002 with increasing depth into the Cambrian (Fig. 4; Clark et al., 2013). The elevated R/R_A values below the Cobourg Formation limestone were interpreted by Clark et al. (2013) to reflect allochthonous fluids of mixed basin and shield origin.

Furthermore, $^{87}Sr/^{86}Sr$ data were reported by Clark et al. (2010a; 2010b) for porewater samples obtained at varying depths in the sedimentary succession. Porewater samples from the Ordovician shales yielded uniform Sr-isotope compositions (mean $^{87}Sr/^{86}Sr$ value of ~0.710) that are enriched in radiogenic Sr relative to the seawater curve of Veizer et al. (1999). Similar to the interpretation of the He isotope data, Clark et al. (2010a; 2010b) considered the ^{87}Sr enrichment to have resulted from *in situ* ingrowth by decay of ^{87}Rb in the porewater. Porewater samples from the Trenton and Black River group limestones yielded highly variable $^{87}Sr/^{86}Sr$ values, between 0.7093 and 0.7103, and consistent with the He-isotope data, were interpreted as resulting from mixing between basin- and shield-derived fluids.

The isotopic and fluid inclusion data from secondary minerals are generally consistent with the conceptual model for porewater evolution presented by Clark et al. (2013) and Al et al. (2015), but our new data allow for some refinements to the model. Based on the porewater data, Clark et al. (2013) and Al et al. (2015) suggest that mixing between basin- and shield-derived fluids was driven by diffusion, but the secondary mineral data indicate that advection in small fractures also contributed to upward transport of shield-type, halite-saturated fluids during stages I to III. These events formed the secondary vein minerals and are broadly constrained by U-Pb dating (Davis, 2013) to the Late Ordovician or Silurian. The isotopic signature of the shield end member does not extend upward into the Trenton Group, likely because it was eliminated by fluid–rock interaction. The fact that present-day porewater in the Black River Group is below halite saturation is consistent with indications of

allochthonous porewater from $^{87}Sr/^{86}Sr$ and $^{3}He/^{4}He$ ratios, and likely reflects the later stages (V to VI) of halite-undersaturated fluid migration that are not recorded in the chemical and isotopic composition of the vein minerals.

6. Conclusions

Overall, the combined microthermometric and isotopic data allow us to establish a model for the fluid migration history associated with the formation of secondary vein minerals in low-permeability Ordovician limestones of the Michigan Basin. Six stages of fluid migration are suggested by the fluid inclusion data. These comprise fluid stages I through III, which are represented by primary inclusions trapped during the formation of dolomite (stage I: 88–128 °C), calcite (stage II: 54–78 °C) and celestine/anhydrite (stage III: 42–80 °C). The ubiquitous presence of variable amounts of halite in these fluid inclusions indicates that the secondary vein minerals precipitated from halite-saturated brines with salinities of 31–37 wt% $[CaCl_2+NaCl]_{eq}$, and is suggestive of a paragenetic link between fluid stages I–III.

Secondary, stage IV inclusions in calcite have a similar, halite-saturated fluid composition as stages I–III, but were trapped above 57–106 °C. No new secondary vein minerals formed during this stage and dissolution features are absent from pre-existing secondary minerals. Stages V and VI represent the latest recognized fluid migrations in the sample suite, during which a halite-undersaturated brine (23–26 wt% $[CaCl_2+NaCl]_{eq}$) was trapped at temperatures < 70 °C.

Secondary minerals from the Cambrian and Shadow Lake units are characterized by the lowest $\delta^{13}C$ and $\delta^{18}O$ values in the succession and $^{87}Sr/^{86}Sr$ ratios that reflect formation from radiogenic Sr sources. The combined Cambrian–Shadow Lake isotopic data are suggestive of secondary mineral formation from hydrothermal brines that experienced high degrees of fluid–rock interaction with the underlying shield, and/or with shield-derived minerals in the Cambrian sandstone. For the Coboconk and Gull River formations, greater variability in the $\delta^{18}O$ and $^{87}Sr/^{86}Sr$ values of the secondary minerals is interpreted to reflect mixed fluid sources, including connate fluids and hydrothermal brines, with the latter having a shield signature sourced from below. Uniform C- O- and Sr-isotope compositions for Trenton Group samples are suggestive of secondary mineral formation from either connate fluids, which were sourced directly from Late Ordovician seawater (or ^{18}O-enriched, evolved seawater), or mixed with hydrothermal brines that underwent high degrees of fluid–rock interaction.

Age constraints on the absolute timing of secondary mineral formation (stages I–III) are gleaned from previous geochronology studies in the region, which indicate that brine influx occurred during the Late Ordovician to Silurian. Secondary inclusions associated with fluid stage IV– which did not form new secondary vein minerals – are interpreted as re-mobilization and/or minor fluid migration along grain boundaries and micro-fractures during a regional heating event. The timing of this regional heating event cannot be easily constrained from our data, however, elsewhere in the Michigan Basin it has been suggested that reactivation of the mid-continent rift during the Late Devonian–Mississippian could be responsible for regional-scale heating and associated fluid migration. Despite evidence elsewhere in the Michigan Basin for secondary-mineral formation during the Late Devonian–Mississippian, the Ordovician limestones at the Bruce site show no evidence of large-scale fluid ingress during this time period (e.g., dissolution/re-precipitation features, formation of new secondary vein minerals); which suggests that the low permeability nature of these rocks had been established before this time.

Acknowledgements

We are grateful to Paul Middlestead, Wendy Abdi and Patricia Wickham for assistance in the G.G. Hatch Stable Isotope Laboratory (uOttawa), and to Douglas Hall and Steven Cogswell for help with EPMA and SEM work at the University of New Brunswick. Shuangquan Zhang, E.A. Spencer and Rhea Mitchell are acknowledged for their assistance with Sr-isotope work in the Isotope Geochemistry and Geochronology Research Centre (Carleton). Rita Caldas kindly assisted with initial microthermometry. We gratefully acknowledge Ian Clark and Josué Jautzy (uOttawa) for discussions on fluid migration models in the Michigan Basin. We are also grateful to Don Davis and Chelsea Sutcliffe (U of T) for thoughtful discussions on the absolute timing of calcite vein emplacement in the Ordovician carbonates. Editor Michael Kersten, an anonymous reviewer and Laura Kennell-Morrison and Richard Crowe (NWMO) are thanked for comments and suggestions on an earlier version of the manuscript. Financial support for this project was provided by the NWMO and NSERC, through an NSERC Industrial Postgraduate Scholarship to JS and an NSERC/NWMO Collaborative Research and Development grant (477852-14) held by TA.

Appendix A. Supplementary data

Supplementary data related to this article can be found at https://doi.org/10.1016/j.apgeochem.2017.09.011.

References

Al, T.A., Clark, I.D., Kennell, L., Jensen, M., Raven, K.G., 2015. Geochemical evolution and residence time of porewater in low-permeability rocks of the Michigan Basin. Southwest Ont. Chem. Geol. 404, 1–17. https://doi.org/10.1016/j.chemgeo.2015.03.005.

Allan, J.R., Wiggins, W.D., 1993. Dolomite reservoirs: geochemical techniques for evaluating origin and distribution. Am. Assoc. Petrol. Geol. Cont. Educ. Course Note Ser. 36.

Altmann, S., Tournassat, C., Goutelard, F., Parneix, J.-C., Gimmi, T., Maes, N., 2012. Diffusion-driven transport in clayrock formations. Appl. Geochem 27, 463–478. https://doi.org/10.1016/j.apgeochem.2011.09.015.

Armstrong, D.K., Carter, T.R., 2010. The Subsurface Paleozoic Stratigraphy of Southern Ontario. Ontario Geological Survey, Special Volume 7.

Arthur, M.A., Cole, D.R., 2014. Unconventional hydrocarbon resources: prospects and problems. ELEMENTS 10, 257–264. https://doi.org/10.2113/gselements.10.4.257.

Ayalon, A., Longstaffe, F.J., 1988. Oxygen isotope studies of diagenesis and porewater evolution in the Western Canada sedimentary basin; evidence from the Upper Cretaceous basal Belly River Sandstone, Alberta. J. Sediment. Res. 58, 489–505. https://doi.org/10.1306/212F8DCD-2B24-11D7-8648000102C1865D.

Beauheim, R.L., Roberts, R.M., Avis, J.D., 2014. Hydraulic testing of low-permeability silurian and ordovician strata, Michigan basin, southwestern Ontario. J. Hydrol. 509, 163–178. https://doi.org/10.1016/j.jhydrol.2013.11.033.

Benson, S.M., Cole, D.R., 2008. CO2 sequestration in deep sedimentary formations. ELEMENTS 4, 325–331. https://doi.org/10.2113/gselements.4.5.325.

Bottomley, D.J., Clark, I.D., 2004. Potassium and boron co-depletion in Canadian Shield brines: evidence for diagenetic interactions between marine brines and basin sediments. Chem. Geol. 203, 225–236. https://doi.org/10.1016/j.chemgeo.2003.10.010.

Bottomley, D.J., Katz, A., Chan, L.H., Starinsky, A., Douglas, M., Clark, I.D., Raven, K.G., 1999. The origin and evolution of Canadian Shield brines: evaporation or freezing of seawater? New lithium isotope and geochemical evidence from the Slave craton. Chem. Geol. 155, 295–320. https://doi.org/10.1016/S0009-2541(98)00166-1.

Clark, I.D., Al, T., Jensen, M., Kennell, L., Mazurek, M., Mohapatra, R., Raven, K.G., 2013. Paleozoic-aged brine and authigenic helium preserved in an Ordovician shale aquiclude. Geology 41, 951–954. https://doi.org/10.1130/G34372.1.

Clark, I.D., Ilin, D., Jackson, R.E., Jensen, M., Kennell, L., Mohammadzadeh, H., Poulain, A., Xing, Y.P., Raven, K.G., 2015. Paleozoic-aged microbial methane in an Ordovician shale and carbonate aquiclude of the Michigan Basin, southwestern Ontario. Org. Geochem. 83–84, 118–126. https://doi.org/10.1016/j.orggeochem.2015.03.006.

Clark, I.D., Mohapatra, R., Mohammadzadeh, H., Kotzer, T., 2010a. Porewater and Gas Analyses in DGR-1 and DGR-2 Core. NWMO Technical Report TR-07-21. Nuclear Waste Management Organization (NWMO), Toronto, p. 25. https://www.nwmo.ca/en/Reports.

Clark, I.D., Liu, I., Mohammadzadeh, H., Zhang, P., Wilk, M., 2010b. Porewater and Gas Analyses in DGR-3 and DGR-4 Core. NWMO Technical Report TR-08-19. Nuclear Waste Management Organization (NWMO), Toronto, p. 29. https://www.nwmo.ca/en/Reports.

Coniglio, M., Williams-Jones, A.E., 1992. Diagenesis of ordovician carbonates from the north-east Michigan basin, Manitoulin Island area, Ontario - evidence from petrography, stable isotopes and fluid inclusions. Sedimentology 39, 813–836. https://doi.org/10.1111/j.1365-3091.1992.tb02155.x.

Coniglio, M., Sherlock, R., Williams Jones, A.E., Middleton, K., Frape, S.K., 1994. Burial and hydrothermal diagenesis of ordovician carbonates from the Michigan basin, Ontario, Canada. In: Purser, B., Tucker, M., Zenger, D. (Eds.), Dolomites a Volume in Honour of Dolomieu. Special Publications of the International Association of Sedimentologists 21. Blackwell Publishing Ltd., Oxford, UK, pp. 231–254. https://doi.org/10.1002/9781444304077.ch14.

Davies, G.R., Smith Jr., L.B., 2006. Structurally controlled hydrothermal dolomite reservoir facies: an overview. Am. Assoc. Petrol. Geol. Bull. 90, 1641–1690. https://doi.org/10.1306/05220605164.

Davis, D.W., 2013. Application of U-Pb Geochronology Methods to the Absolute Age Determination of Secondary Calcite. NWMO Technical Report TR-2013-21. Nuclear Waste Management Organization (NWMO), Toronto, p. 31. https://www.nwmo.ca/en/Reports.

Davis, D.W., Sutcliffe, C.N., Smith, P., Zajacz, Z., Thibodeau, A.M., Spalding, J., Schneider, D., Adams, J., Cruden, A. and Parmenter, A., 2017. Secondary calcite as a useful U-Pb geochronometer: An example from the Paleozoic sedimentary sequence in southern Ontario. GAC-MAC 2017 Joint Annual Meeting, Kingston, ON, Canada, May 14–18. Abstracts Volume.

Diamond, L.W., 2003. Systematics of H_2O inclusions. In: Samson, I.M., Anderson, A.J., Marshall, D.D. (Eds.), Short Course 32. Fluid Inclusions: Analysis and Interpretation. Short Course 32. Mineralogical Association of Canada, pp. 55–79.

Diamond, L.W., Aschwanden, L., Caldas, R., 2015. Fluid Inclusion Study of Core and Outcrop Samples from the Bruce Nuclear Site, Southern Ontario, Canada. NWMO Technical Report TR-2015-24. Nuclear Waste Management Organization (NWMO), Toronto, p. 138. https://www.nwmo.ca/en/Reports.

Douglas, M., Clark, I.D., Raven, K., Bottomley, D., 2000. Groundwater mixing dynamics at a Canadian Shield mine. J. Hydrol. 235, 88–103. https://doi.org/10.1016/S0022-1694(00)00265-1.

Frape, S.K., Fritz, P., McNutt, R.H., 1984. Water-rock interaction and chemistry of groundwaters from the Canadian Shield. Geochim. Cosmochim. Acta 48, 1617–1627. https://doi.org/10.1016/0016-7037(84)90331-4.

Friedman, I., O'Neil, J.R., 1977. Compilation of Stable Isotope Fractionation Factors of Geochemical Interest. USGS Professional Paper 440-KK.

Fritz, P., Frape, S.K., 1982. Saline groundwaters in the Canadian Shield — a first overview. Chem. Geol. 36, 179–190. https://doi.org/10.1016/0009-2541(82)90045-6.

Gascoyne, M., 2004. Hydrogeochemistry, groundwater ages and sources of salts in a granitic batholith on the Canadian Shield, southeastern Manitoba. Appl. Geochem 19, 519–560. https://doi.org/10.1016/S0883-2927(03)00155-0.

Girard, J.-P., Barnes, D.A., 1995. Illitization and paleothermal regimes in the Middle ordovician St. Peter sandstone, central Michigan basin: K-Ar, oxygen isotope, and fluid inclusion data. Am. Assoc. Petrol. Geol. Bull. 79, 49–69.

Goldstein, R.H., 2001. Fluid inclusions in sedimentary and diagenetic systems. Lithos 55, 159–193. https://doi.org/10.1016/S0024-4937(00)00044-X.

Goldstein, R.H., Reynolds, T.J., 1994. Systematics of Fluid Inclusions in Diagenetic Minerals. SEPM (Society for Sedimentary Geology) Short Course 31, Tulsa, U.S.A.

Haeri-Ardakani, O., Al-Aasm, I., Coniglio, M., 2013. Fracture mineralization and fluid flow evolution: an example from Ordovician-Devonian carbonates, southwestern Ontario, Canada. Geofluids 13, 1–20. https://doi.org/10.1111/gfl.12003.

Hanor, J.S., 2001. Reactive transport involving rock-buffered fluids of varying salinity. Geochim. Cosmochim. Acta 65, 3721–3732. https://doi.org/10.1016/S0016-7037(01)00703-7.

Harper, D.A., Longstaffe, F.J., Wadleigh, M.A., McNutt, R.H., 1995. Secondary K-feldspar at the precambrian–paleozoic unconformity, southwestern Ontario. Can. J. Earth Sci. 32, 1432–1450. https://doi.org/10.1139/e95-116.

Hendry, M.J., Solomon, D.K., Person, M., Wassenaar, L.I., Gardner, W.P., Clark, I.D., Mayer, K.U., Kunimaru, T., Nakata, K., Hasegawa, T., 2015. Can argillaceous formations isolate nuclear waste? Insights from isotopic, noble gas, and geochemical profiles. Geofluids 15, 381–386. https://doi.org/10.1111/gfl.12132.

Holser, W.T., 1979. Mineralogy of evaporites. In: Burns, R.G. (Ed.), Marine Minerals. Reviews in Mineralogy and Geochemistry, vol. 6. Mineralogical Society of America, pp. 295–346.

Horita, J., 2014. Oxygen and carbon isotope fractionation in the system dolomite-water-CO_2 to elevated temperatures. Geochim. Cosmochim. Acta 129, 111–124. https://doi.org/10.1016/j.gca.2013.12.027.

Hurley, N.F., Budros, R., 1990. Albion-scipio and stoney point Fields-U.S.A., Michigan basin. Am. Assoc. Petrol. Geol. Special Volumes 23, 1–37.

Intera, 2011. Descriptive Geosphere Site Model. NWMO Technical Report TR-2011-24. Nuclear Waste Management Organization (NWMO), Toronto, p. 426. http://www.nwmo.ca/dgrgeoscientificsitecharacterization.

Khader, O., Novakowski, K., 2014. The Study of Diffusion Dominant Solute Transport in Solid Host Rock for Nuclear Waste Disposal. Report to: Canadian Nuclear Safety Commission).

Knauth, L.P., Beeunas, M.A., 1986. Isotope geochemistry of fluid inclusions in Permian halite with implications for the isotopic history of ocean water and the origin of saline formation waters. Geochim. Cosmochim. Acta 50, 419–433. https://doi.org/10.1016/0016-7037(86)90195-X.

Kyser, T., Kerrich, R., 1990. Geochemistry of fluids in tectonically active crustal regions. Short course on fluids in tectonically active regimes of the continental crust. Mineral Assoc. Can. Short Course Handb. 18, 133–230.

Legall, F.D., Barnes, C.R., Macqueen, R.W., 1981. Thermal maturation, burial history and hotspot development, paleozoic strata of southern Ontario - quebec, from conodont and acritarch colour alteration studies. Bull. Can. Petrol. Geol. 29, 492–539.

Ma, L., Castro, M.C., Hall, C.M., 2009. Atmospheric noble gas signatures in deep Michigan Basin brines as indicators of a past thermal event. Earth Planet. Sci. Lett. 277, 137–147. https://doi.org/10.1016/j.epsl.2008.10.015.

Mazurek, M., de Haller, A., 2017. Pore-water evolution and solute-transport mechanisms in opalinus clay at mont terri and mont russelin (canton jura, Switzerland). Swiss J. Geosci. 110, 129–149. https://doi.org/10.1007/s00015-016-0249-9.

McNutt, R.H., Frape, S.K., Fritz, P., 1984. Strontium isotopic composition of some brines from the Precambrian Shield of Canada. Chem. Geol. 46, 205–215. https://doi.org/10.1016/0009-2541(84)90190-6.

Middleton, K., Coniglio, M., Frape, S.K., 1993. Dolomitization of Middle ordovician carbonate reservoirs, southwestern Ontario. Bull. Can. Petrol. Geol. 41, 150–163.

Neuzil, C.E., Provost, A.M., 2014. Ice sheet load cycling and fluid underpressures in the Eastern Michigan Basin, Ontario, Canada. J. Geophys. Res. Solid Earth 119, 8748–8769. https://doi.org/10.1002/2014JB011643.

Neuzil, C.E., 2015. Interpreting fluid pressure anomalies in shallow intraplate argillaceous formations. Geophys. Res. Lett. 42, 4801–4808. https://doi.org/10.1002/2015GL064140.

Normani, S.D., Sykes, J.F., 2012. Paleohydrogeologic simulations of Laurentide ice-sheet history on groundwater at the eastern flank of the Michigan Basin. Geofluids 12, 97–122. https://doi.org/10.1111/j.1468-8123.2012.00362.x.

NWMO, 2011. Geosynthesis. NWMO Technical Report TR-2011-11. Nuclear Waste Management Organization (NWMO), Toronto, p. 418. https://www.nwmo.ca/en/Reports.

Oakes, C.S., Bodnar, R.J., Simonson, J.M., 1990. The system NaCl-$CaCl_2$-H_2O: I. The ice liquidus at 1 atm total pressure. Geochim. Cosmochim. Acta 54, 603–610. https://doi.org/10.1016/0016-7037(90)90356-P.

Obermajer, M., Fowler, M.G., Snowdon, L.R., 1999. Depositional environment and oil generation in Ordovician source rocks from southwestern Ontario, Canada: organic geochemical and petrological approach. Am. Assoc. Petrol. Geol. Bull. 83, 1426–1453.

Ontario Geological Survey, 1991. Bedrock Geology of Ontario, Southern Sheet. Ontario Geological Survey. Map 2544, Scale 1:1,000,000.

Pearson Jr., F.J., 1987. Models of mineral controls on the composition of saline groundwaters of the Canadian Shield. Geol. Assoc. Can. - Special Pap. 33, 39–51.

Powell, T.G., Macqueen, R.W., Barker, J.F., Bree, D.G., 1984. Geochemical character and origin of Ontario oils. Bull. Can. Petrol. Geol. 32, 289–312.

Roedder, E., 1984. Fluid inclusions. In: Ribbe, P.E. (Ed.), Reviews in Mineralogy and Geochemistry, vol. 12. Mineralogical Society of America (Reviews in Mineralogy and Geochemistry, Mineral Soc Am.).

Roedder, E., 1979. Fluid Inclusion Evidence on the Environments of Sedimentary Diagenesis, a Review. The Society of Economic Paleontologists and Mineralogists, Special Publication, pp. 89–107.

Roedder, E., Bodnar, R.J., 1980. Geologic pressure determinations from fluid inclusion studies. Annu. Rev. Earth Planet. Sci. 8, 263–301.

Russell, D.J., Gale, J.E., 1982. Radioactive waste disposal in the sedimentary rocks of southern Ontario. Geosci. Can. 9, 200–207.

Samson, I.M., Anderson, A.J., Marshall, D.D., 2003. Fluid Inclusions: Analysis and Interpretation. Mineralogical Association of Canada. Short Course 32.

Saso, J., 2013. Paleohydrogeological Investigation of Upper Ordovician and Cambrian Rocks from the Michigan Basin in Southwestern Ontario. University of New Brunswick (M.Sc. Thesis).

Shafeen, A., Croiset, E., Douglas, P., Chatzis, I., 2004. CO2 sequestration in Ontario, Canada. Part I: storage evaluation of potential reservoirs. Energy Convers. Manag. 45, 2645–2659.

Shields, G.A., Carden, G.A.F., Veizer, J., Meidla, T., Rong, J.-Y., Li, R.-Y., 2003. Sr, C, and O isotope geochemistry of Ordovician brachiopods: a major isotopic event around the Middle-Late Ordovician transition. Geochim. Cosmochim. Acta 67, 2005–2025. https://doi.org/10.1016/S0016-7037(02)01116-X.

Spencer, R.J., 1987. Origin of CaCl brines in Devonian formations, western Canada sedimentary basin. Appl. Geochem 2, 373–384. https://doi.org/10.1016/0883-2927(87)90022-9.

Steele-MacInnis, M., Bodnar, R.J., Naden, J., 2011. Numerical model to determine the composition of H_2O–NaCl–$CaCl_2$ fluid inclusions based on microthermometric and microanalytical data. Geochim. Cosmochim. Acta 75, 21–40. https://doi.org/10.1016/j.gca.2010.10.002.

Taylor, T.R., Sibley, D.F., 1986. Petrographic and geochemical characteristics of dolomite types and the origin of ferroan dolomite in the Trenton Formation, Ordovician, Michigan Basin, U.S.A. Sedimentology 33, 61–86. https://doi.org/10.1111/j.1365-3091.1986.tb00745.x.

Veizer, J., Ala, D., Azmy, K., Bruckschen, P., Buhl, D., 1999. 87Sr/86Sr, $\delta^{13}C$ and $\delta^{18}O$ evolution of Phanerozoic seawater. Chem. Geol. https://doi.org/10.1016/S0009-2541(99) 00081–00089.

Wickstrom, L.H., Gray, J.D., Stieglitz, R.D., 1992. Stratigraphy, Structure, and Production History of the Trenton Limestone (Ordovician) and Adjacent Strata in Northwestern Ohio. Rep. of investigations/State of Ohio. Dep. of natural resources, Div. of geol. survey. https://doi.org/10.1111/j.1502-3931.1996.tb01833.x/full.

Wilson, T.P., Long, D.T., 1993a. Geochemistry and isotope chemistry of CaNaCl brines in Silurian strata, Michigan Basin, U.S.A. Appl. Geochem. 8, 507–524. https://doi.org/10.1016/0883-2927(93)90079-V.

Wilson, T.P., Long, D.T., 1993b. Geochemistry and isotope chemistry of Michigan Basin brines: Devonian formations. Appl. Geochem 8, 81–100. https://doi.org/10.1016/0883-2927(93)90058-O.

Ziegler, K., Longstaffe, F.J., 2000. Multiple episodes of clay alteration at the precambrian/paleozoic unconformity, Appalachian Basin: isotopic evidence for long- distance and local fluid migrations. Clays Clay Minerals 48, 474–493. https://doi.org/10.1021/ac60068a025.